Science of the Total Environment 723 (2020) 138088

Contents lists available at ScienceDirect

Science of the Total Environment

journal homepage: www.elsevier.com/locate/scitotenv

Diagenetic production, accumulation and sediment-water exchanges of methylmercury in contrasted sediment facies of Lake Titicaca (Bolivia)

S. Guédron [a,b,*], S. Audry [c], D. Acha [d], S. Bouchet [e,1], D. Point [c], T. Condom [f], C. Heredia [a,d], S. Campillo [a], P.A. Baya [c], A. Groleau [g], E. Amice [h], D. Amouroux [d,e]

[a] Univ. Grenoble Alpes, Univ. Savoie Mont Blanc, CNRS, IRD, IFSTTAR, ISTerre, 38000 Grenoble, France
[b] Laboratorio de Hidroquímica, Instituto de Investigaciones Químicas, Universidad Mayor de San Andres, Campus Universitario de Cota Cota, casilla 3161, La Paz, Bolivia
[c] Géosciences Environnement Toulouse, UMR5563, IRD UR 154, Université Paul Sabatier, 14 Avenue Edouard Belin, 31400 Toulouse, France
[d] Unidad de Calidad Ambiental (UCA), Instituto de Ecología, Universidad Mayor de San Andrés, Campus Universitario de Cota Cota, casilla 3161, La Paz, Bolivia
[e] Universite de Pau et des Pays de l'Adour, E2S UPPA, CNRS, IPREM, Institut des Sciences Analytiques et de Physico-chimie pour l'Environnement et les matériaux, Pau, France
[f] Univ. Grenoble Alpes, CNRS, IRD, Grenoble INP, Institut des Géosciences de l'Environnement (IGE), UMR 5001, F-38000 Grenoble, France
[g] Institut de Physique du Globe de Paris (IPGP), 1, rue Jussieu, 75238 Paris Cedex 05, France
[h] LEMAR- Laboratoire des sciences de l'environnement marin, Institut Universitaire Européen de la Mer - Technopôle Brest-Iroise, Rue Dumont d'Urville, 29280 Plouzané, France

HIGHLIGHTS

- Mercury (Hg) speciation was analyzed in Lake Titicaca sediment cores.
- Monomethymercury (MMHg) accounted for up to 90% of total Hg in porewater (PW).
- Highest MMHg accumulation in PW was found in carbonate-rich sediment.
- The iron-sulfide loop and organic matter controlled Hg and MMHg accumulation in PW.
- MMHg sediment diffusive flux contributed to over 1/3 of MMHg load in the water column.

GRAPHICAL ABSTRACT

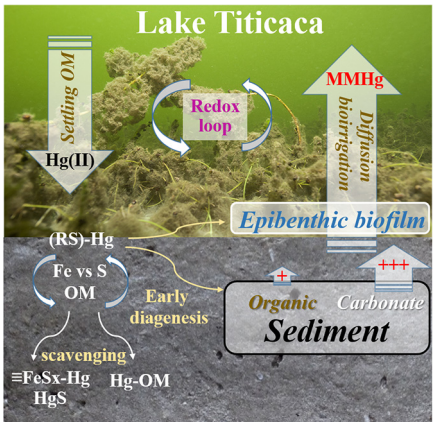

ARTICLE INFO

Article history:
Received 9 December 2019
Received in revised form 18 March 2020
Accepted 19 March 2020
Available online 21 March 2020

Editor: Mae Sexauer Gustin

Keywords:
Methylmercury
Lake sediment

ABSTRACT

Monomethylmercury (MMHg) concentrations in aquatic biota from Lake Titicaca are elevated although the mercury (Hg) contamination level of the lake is low. The contribution of sediments to the lake MMHg pool remained however unclear. In this work, seven cores representative of the contrasted sediments and aquatic ecotopes of Lake Titicaca were sliced and analyzed for Hg and redox-sensitive elements (Mn, Fe, N and S) speciation in pore-water (PW) and sediment to document early diagenetic processes responsible for MMHg production and accumulation in PW during organic matter (OM) oxidation.

The highest MMHg concentrations (up to 12.2 ng L^{-1} and 90% of THg) were found in subsurface PWs of the carbonate-rich sediments which cover 75% of the small basin and 20% of the large one. In other sediment facies, the larger content of OM restricted MMHg production and accumulation in PW by sequestering Hg in the solid

* Corresponding author at: ISTerre, Université Grenoble Alpes, Institut de Recherche pour le Développement (IRD), UMR 5275 (IRD/UGA/CNRS), BP 53, F-38041 Grenoble, France.
E-mail address: stephane.guedron@ird.fr (S. Guédron).
[1] Present address: Eawag, Swiss Federal Institute of Aquatic Science and Technology, CH-8600 Dübendorf, Switzerland and ETH Zürich, Universitätstrasse 16, CH-8092 Zürich, Switzerland.

https://doi.org/10.1016/j.scitotenv.2020.138088

Early diagenesis
High altitude ecosystem
Diffusive fluxes

phase and potentially also by decreasing its bioavailability in the PW. Diagenetically reduced S and Fe played a dual role either favoring or restricting the availability of Hg for biomethylation.
The calculation of theoretical diffusive fluxes suggests that Lake Titicaca bottom sediments are a net source of MMHg, accounting for more than one third of the daily MMHg accumulated in the water column of the Lago Menor. We suggest that in the context of rising anthropogenic pressure, the enhancement of eutrophication in high altitude Altiplano lakes may increase these MMHg effluxes into the water column and favor its accumulation in water and biota.

1. Introduction

Lake sediment is known to be an important sink for inorganic mercury but can be a source of neurotoxic monomethylmercury (MMHg) for their overlying waters (Fitzgerald et al., 2014), in which trophic transfer occurs in both benthic and pelagic organisms (Watras et al., 1998; García Bravo et al., 2014; Gimbert et al., 2016). Biogeochemical processes involved in the methylation of mercury (Hg) generally occur in surficial sediment or biofilms developed at the sediment/water interface (SWI) and imply various micro-organisms amongst which the most documented are methanogens, sulfate-reducing (SRB) and iron-reducing (IRB) bacteria (Acha et al., 2005; Kerin et al., 2006; Hamelin et al., 2014; Garcia Bravo et al., 2015). Such processes occur specifically during early diagenesis, when part of the deposited fresh organic matter (OM) is oxidized close to the SWI, with O_2, NO_3^-, Mn- and Fe-oxy(hydr)oxides or SO_4^{2-} acting as electron acceptors (Froelich et al., 1979; De Lange, 1986; Meyers and Ishiwatari, 1993). In anoxic sediments, Hg (II) and MMHg are associated with sulfidized OM (Skyllberg, 2008) or authigenic Fe sulfide minerals, and to a minor extent precipitated as cinnabar (HgS(s) and montroydite (HgO(s)) (Hammerschmidt and Fitzgerald, 2004; Sunderland et al., 2006; Jeong et al., 2007; Merritt and Amirbahman, 2007; Liu et al., 2008; Hollweg et al., 2009; Feyte et al., 2012; Guédron et al., 2012). While Hg is reported to be conservative in sediment cores, MMHg generally declines with sediment depth due to demethylation (Hines et al., 2004; Rydberg et al., 2008) making difficult the use of MMHg concentration in sediment as an historical record of lake MMHg production.

In the high altitude Bolivian Altiplano (above 3700 m a.s.l.), high percentages of MMHg were reported in the water column rising from <1 up to ~50% of total mercury (THg) from the oligo/hetero-trophic Lake Titicaca to the eutrophic Lake Uru-Uru (Alanoca et al., 2016b; Guédron et al., 2017). Although anthropogenically induced eutrophication is reported to favor MMHg accumulation in the water column (Acha et al., 2018), variations of MMHg concentrations in surface water are also affected by parameters varying on a daily basis (e.g., temperature, oxygen) that can overwhelm seasonal variations (Amouroux et al., 2015; Alanoca et al., 2016a). Furthermore, the sediment is a likely major source of MMHg for the water column but has been poorly documented yet in these lakes.

In the shallow Lake Uru-Uru, the quantification of methylation potentials during incubations experiments with enriched isotopes, revealed that sediments represented a major source of MMHg for the water column (Alanoca et al., 2016a). In contrast, same experiments in Lake Titicaca indicated intense methylation in epibenthic biofilms and periphyton associated with emerged macrophytes compared to sediments and submerged aquatic plants' periphyton (Bouchet et al., 2018). However, the area covered by sediments is such that they may significantly contribute to the MMHg pool in the water column of Lake Titicaca. Such exchanges strongly depend on molecular diffusion and physical advection rates of dissolved species which are controlled by the stratification of the sediment/water interface (SWI) and resuspension resulting from sustained winds and shear stress (e.g., during storm events) especially in shallow environments (Schäfer et al., 2010; Guédron et al., 2012; Bouchet et al., 2013). Amongst the physico-chemical factors that regulate the intensity of Hg and MMHg diffusive fluxes are; (i) the steepness of the concentration gradient and the position of the redox front around the SWI (Hammerschmidt and Fitzgerald, 2008), (ii) the abundance and type of (in)organic ligands (Skyllberg, 2008; Bouchet et al., 2018) and colloids (Guédron et al., 2016), and (iii) the sediment structure (e.g., porosity, tortuosity). Furthermore, benthic fluxes can be enhanced by bioirrigation (e.g., benthic organisms) creating preferential water pathways in the sediment at the SWI (Point et al., 2007; Benoit et al., 2009).

To document the geochemical post-depositional fate and behavior of (MM)Hg in the high-altitude Lake Titicaca, we studied in high resolution (5 to 20 mm-vertical scale) the speciation of Hg together with redox-sensitive elements (N, Mn, Fe and S species) in seven sediment cores representative of the various lake sediment facies and Hg contamination levels. We also calculated Hg and MMHg diffusive fluxes at the SWI to assess the MMHg contribution of each sediment facies toward the water column at different spatial and temporal scales.

2. Background information and methods

2.1. General settings

2.1.1. Lake Titicaca

Located in the central Andean Altiplano (a high endorheic plateau in Peru and Bolivia), Lake Titicaca (surface = 8562 km^2; volume = 903 km^3) is the largest navigable water body in the world lying at an altitude of 3809 m above sea level (Dejoux, 1992). Lake water is alkaline with a salinity close to 1 g L^{-1} with elevated sulfate concentrations [~300 mg L^{-1}, (Dejoux, 1992)]. The seasonal cycle of rainfall is marked, with the rainy season concentrated between December and March (Segura et al., 2019). The lake is composed of two main water bodies, the Lago Mayor (or Chucuito ~7092 km^2) and The Lago Menor [or Huiñaimarca ~1470 km^2 (Dejoux, 1992)]. The Lago Menor makes up only ~16% of the area of Lake Titicaca and is characterized by a shallow mean depth (~9 m) and a large area at <5 m in depth (~56% of the surface). Its slopes are very gentle and the current flows from the Lago Mayor at the Tiquina straight to the Desaguadero, its outflow. Three main bathymetrical zones are differentiated in the Lago Menor; (i) the deepest zone down to 41 m in the North, known as the Chua trough, (ii) a central basin in the center west beyond the line of islands with a maximum depth of 20 m and (iii) a shallow area extending between and around these two zones, with a sill about 7 m deep between the Chua trough and the central depression (Fig. 1).

Levels of THg in water and sediment of Lake Titicaca are in the lowest range of reported levels in other large lakes worldwide (Guédron et al., 2017). The main Hg loading sources to the lake are natural atmospheric wet and dry deposition and catchment eroded particles (Guédron et al., 2017; Guédron et al., 2018). Only a few Hg point sources including current and historical mining (e.g., Ramis, Suchez) and urban areas (e.g., El Alto and Puno) impact the lake locally (Archundia et al., 2017; Guédron et al., 2017).

2.1.2. Benthic ecology and sediment facies of Lake Titicaca

Emerged macrophytes are the most abundant plant group in Lake Titicaca, with a third of the bottom colonized by *Characeae* (*Chara spp.*), representing around 436 km^2 in Lago Menor [~60% of the area

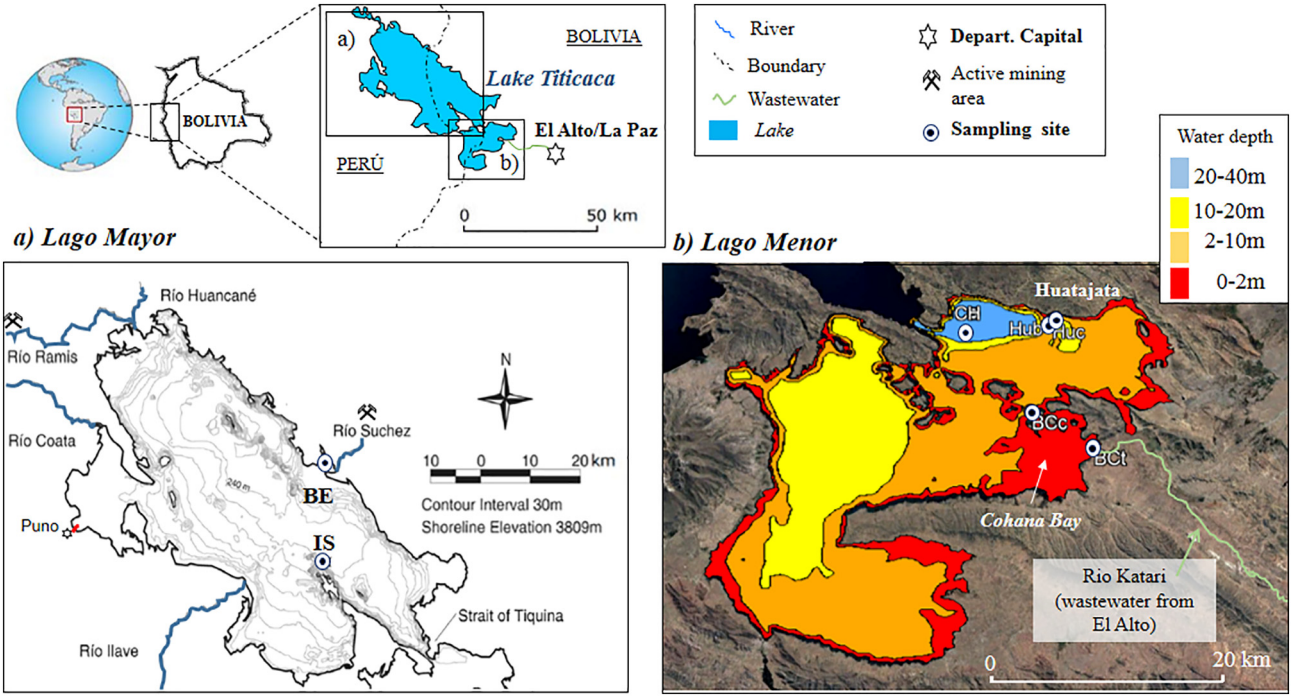

Fig. 1. Top panel: location of the two sub-basins of Lake Titicaca at the frontier between Peru and Bolivia. Bottom panels: Map of Lake Titicaca including the two sub-basins a) Lago Mayor with Escoma Bay (BE) and Sun Island (IS) sampling sites and b) Lago Menor with Huatajata (HU; cores HUb and HUc), Chua (CH), and Cohana Bay (BC; cores BCt and BCc) sampling site location. Note the subscripts given after sampling site names refer to the type of benthic biome covering the sediment with b for biofilms, c for characeae (*Chara spp.*), and t for totoras (*Schoenoplectus totoras*).

covered by vegetation (Collot et al., 1983)]. In the inner margin or shore line (between 0 and 2 m depth), the sedge also called "totoras" (*Schoenoplectus totoras*) are the most abundant aquatic plants. Calcium-fixing *Characeae* occur from the inner margin or even from the shoreline where the totoras are sparse or absent, down to a maximum of 15 m depth. They constitute >60% of the total biomass in Lago Menor and account for ~60% of the primary production (Dejoux, 1993). In deep open water (i.e., above 15 m depth), primary production is dominated by phytoplankton (Dejoux, 1992).

From the primary producers ecological allocation and the distribution of autochthonous (mostly carbonate) and allochthonous (detrital minerals) materials, Lago Menor can be characterized by four main sediment facies (Boulange et al., 1981) defined as follows: (i) the carbonate detrital facies found in the littoral zones, broadly composed of ~ 25% organic matter (OM) and 20 to 70% carbonates, (ii) the carbonate facies composed of ~ 60% carbonates (calcite/aragonite) and < 20% OM encountered in shallow areas (i.e., between 2 and 10 m depth) where *Characeae* are the most abundant, (iii) the organo-detrital of the deep zone (i.e., Chua trough) composed of 25 to 50% OM (derived from plankton decomposition) and < 15% carbonates, and (iv) the organic facies in very shallow areas where totoras are abundant (i.e., < 2 m) composed of >50% OM and between 25 and 45% of detrital fraction.

Despite similarities in sediment facies between the two basins, Lago major is characterized by lower OM and carbonate content (because of the deeper water column and lower aquatic vegetation) and higher detrital sandy fraction (Rodrigo and Wirrmann, 1992). The two most representative facies of this later are the detrital facies (containing >70% of clastic components and <25% OM) and the carbonate detrital facies, while the carbonate facies is only found on the littoral.

2.2. Sediment and water collection

Seven short cores (25 to 30 cm) were sampled during two campaigns (April and October 2014) in areas representative of the lake main sediment facies (Fig. 1 and S.I.1). Three cores were sampled (April and November 2014) in the organo-detritic calcareous sediments or carbonate facies (i.e., between 2 and 10 m depth); two in front of Huatajata village in a shallow area covered by *Characeae* (subscript = c; core HUc: ~7 m depth, 25.04.2014), another covered by epibenthic biofilms (subscript = b; HUb ~8 m depth, 23.04.2014) and a third one at the outlet of the Cohana Bay in a very shallow area covered by *Characeae* (core BCc, 2 m depth, 13.10.2014). A core was collected in the deep Chua trough (Core CH, 38 m depth, 19.04.2014) to recover the organo-detrital facies. A littoral core was collected in the shallow organic facies of the Cohana bay covered by totoras (subscript = t; core BCt; 1.8 m depth, 27.04.2014), an area which receives urban effluents from the city of El Alto (~900,000 inhabitants) flowing through the Katari River (Archundia et al., 2017). Finally, two additional core were collected in the Lago Mayor, the first in the detrital facies of the Escoma Bay potentially exposed to mining effluents from the large mining area located in the upstream watershed of Suchez River (core BE; 26 m depth, 07.10.2014) and the second in the carbonate facies of open lake close to the Sun Island (core IS; 19 m depth, 11.06.2014).

All details and procedure for sediment sampling, slicing and conditioning of sediment and porewater are described in S.I.1 and in Guédron et al. (2017). Briefly, sediments were recovered using a gravity Corer (Uwitec®), extruded and sliced with a vertical resolution of 5 mm near the SWI, up to 2 cm thick near the bottom. Collected overlying water (OW) and porewater (PW) were filtered (0.45 μm porosity; Millipore®) and divided into three aliquots for Hg speciation, anions and major and traces analyses. This filtered fraction encompasses filter passing colloids which may evolve during the filtration procedure in relation with filter clogging (Guédron et al., 2016). To complement the diffusive fluxes between surface sediment PW and OW obtained from collected cores, additional sampling was performed by scuba divers close to the coring sites of HU and BC at various season and time period during the day. Surface porewater water were sampled with 0.8 cm long microporous polymer tube samplers (MicroRhizon®, 0.45 μm porosity; Rhizosphere Research Products) during 2 h following published protocols (Guédron et al., 2011; Guédron et al., 2012). OW were collected few meters away from the PW sampling sites by scuba divers into benthic chambers's sampling setup (Point et al., 2007) at the beginning of

the incubation (within the 50 cm above the sediment interface) with acid washed syringes before the end of the porewater water sampling period (S.I.1).

2.3. Chemical analyses

All details for chemical analysis and QA/QC are given in S.I.2 and in Guédron et al. (2017).

2.3.1. Sediment characterization, conditioning and digestion

Sediment water content and dry bulk density (DBD) were obtained from difference in weight (wet vs freeze-dried) of each slice of sediment. Each freeze-dried sediment slice was ground (<63 μm). Three sediment cores (CH, HUc and BCt) were digested for total elemental concentration and selective extraction. Sediment total digestion were performed using a mixture of H_2O_2/HNO_3/HF (Ultrex grade – Baker) following a published protocol (Guédron et al., 2006). All details for the method, blanks and certified international reference materials are provided in S.I.1. The most reactive Fe and Mn oxide fraction were selectively extracted by an ascorbate reagent (Kostka and Luther, 1994; Anschutz et al., 2000; Guédron et al., 2009). All elemental concentrations in sediment are reported on a dry weight basis.

2.3.2. Major and trace element analysis in digested solids and filtered solutions

Major (Ca, Fe, Al, Mn and S) elements in water and digested sediment were measured by ICP-OES (Varian model 720ES) within the analytical chemistry platform of ISTerre (OSUG-France), trace elements (Mo, U, and Fe and Mn in PW) by quadrupole ICP-MS 7500 ce (Agilent Technologies) within the analytical chemistry platform of UPPA and ascorbate-extractable Fe (Fe_{asc}) and Mn (Mn_{asc}) by flame AAS (Perkin-Elmer AAnalyst 400) within the analytical chemistry platform of GET laboratory. Total sulfur obtained by ICP-AES in digested sediment were intercompared and in good agreement (Fig. S1) with analysis performed by S Elemental analyzer (Flash 2000, Thermo Scientific, Milan, Italy). Major anions concentrations were determined by ion chromatography (Dionex ICS 2000) and hydrogen sulfides by HPLC-UV (S.I. 1).

2.3.3. Total carbon, total organic carbon and their isotopic signatures ($\delta^{13}C$)

Total carbon (TC), total organic carbon (Corg) content and their isotopic composition ($\delta^{13}C_{bulk}$ and $\delta^{13}C_{org}$) were measured by Cavity Ring-Down Spectrometry (Picarro, Inc.®) coupled with Combustion Module (Costech, Inc.®) (CM-CRDS) using previously reported analytical methods, calibration and sample preparation (Paul et al., 2007; Balslev-Clausen et al., 2013; Guédron et al., 2019). More details are supplied in S.I.2.

2.3.4. Hg speciation in solutions and solids

Total mercury concentrations (THg) in filtered water samples were determined by cold vapor atomic fluorescence spectrometry (CV-AFS) after conversion of all mercury species into Hg^0 (Bloom and Fitzgerald, 1988; Cossa et al., 2009) followed by detection using a Tekran® (Model 2500). Total Hg concentrations in sediment were determined by atomic absorption spectrophotometry [Altec, Model AMA 254 (Guédron et al., 2009)].

Monomethylmercury concentrations in water and digested sediments were analyzed using a purge and trap-gas chromatograph-atomic fluorescence spectroscopy analyzer (MERX System, Brooks Rand®) and intercompared by propylation ID-GC–ICPMS (S.I.2.2) following published protocols (Monperrus et al., 2008; Guédron et al., 2014).

2.4. Water/sediment fluxes measurements and calculations

2.4.1. Diffusive fluxes calculation

Molecular diffusion from sediment to overlying water was estimated by calculation of the diffusion fluxes for Hg(II) (with Hg(II) = THg − MMHg) and MMHg at the SWI using the measured concentration gradient and Fick's first law (Berner, 1980; Boudreau, 1996):

$$Jsed = -Ø/Dsed\ (\partial C/\partial z)$$

where Jsed ($ng \cdot m^{-2}\ d^{-1}$) is the diffusive flux in the sediment, Ø porosity, Dsed is the diffusive coefficient in sediment [$2 \times 10^{-6}\ cm^2\ s^{-1}$ and $1.2 \times 10^{-5}\ cm^2\ s^{-1}$ for Hg(II) and MMHg ionic/molecular diffusion coefficient in water (Rothenberg et al., 2008)] and $\partial C/\partial z$ is the linear concentration gradient through the SWI. Details are given in Supplementary information (S.I.4). Positive Jsed indicates an upward-directed flux (efflux from the sediment into the overlying water column) and negative Jsed indicates a downward-directed flux (influx from the water column into the sediment). The total contribution of each sediment facies to the water column was estimated by integrating their Jsed over their respective surface area coverage of the bottom of the lake.

2.4.2. Sediment surface and water volume quantification in Lago Menor

Bathymetric data are issued from the digitalization of the bathymetric map n°3500 (Comision Mixta Peruana Boliviana, 1977). The scale is 1/100.000 in Mercator projection and the lake levels are relative to the lake altitude in that was equal to 3810.4 m a.s.l. The area/volume/depth distributions of the Lago Menor were derived using the following steps realized with ArcGIS©10.3: (i) digitalization of the depth curves; (ii) rasterization of the vector curves to create a 100 by 100 m raster grid; (iii) extraction of the area/depth/volume relations each 1 m using spatial analyst; (iv) separation into 4 classes adapted to the depth cores ([0–2 m]; [2–20 m]; [20–41 m]). The maximum depth is 41 m and is found in the Chua trough, the eastern part of the Lago Minor. All details are given in S.I.2.3.

2.5. Statistical treatment and data presentation

Because geochemical data were not normally distributed, the following parameters are reported: mean, standard deviation (SD), and the number of observations N (Webster, 2001). Correlation coefficient (R) and *P* values (P) are reported for elemental regressions. All statistical analyses were performed using Sigmastat and a *p*-value of 0.05 was chosen to indicate statistical significance.

3. Results

3.1. Carbonate-rich sediment

3.1.1. Carbonate facies of the Lago Menor

The carbonate facies covers approx. 75% of the Lago Menor bottom area (Table S4). The abundant and productive calcium-fixing macrophytes (i.e., *Characeae*) made this sediment facies enriched in carbonates ($CaCO_3$ (mean ± SD) in core HUc = 80 ± 13%, $N = 24$). In opposition, the OM content was low (Corg = 5.5 ± 1.2%, N = 24 in core HUc) with heavy $\delta^{13}C$ signatures (−16.5 ± 0.6‰, N = 24 - Fig. 2a) typical of the submerged macrophytes (*characeae*) from the lake shallows [~12 ± 4‰ (Rowe et al., 2002)]. Detrital components were also low with Fe (0.37 ± 0.05%, N = 24) and Mn (45 ± 4 $\mu g\ g^{-1}$, N = 24)) contents being around 10 times lower than in the sediment of Lake Uru-Uru (2.8 ± 0.5% and 486 ± 114 $\mu g\ g^{-1}$, respectively) located downstream in the endorheic basin (Tapia and Audry, 2013). Reactive Fe (Fe_{asc}) and Mn (Mn_{asc}) were almost constant with depth and never exceeded 5% and 10% of total Fe and Mn concentrations

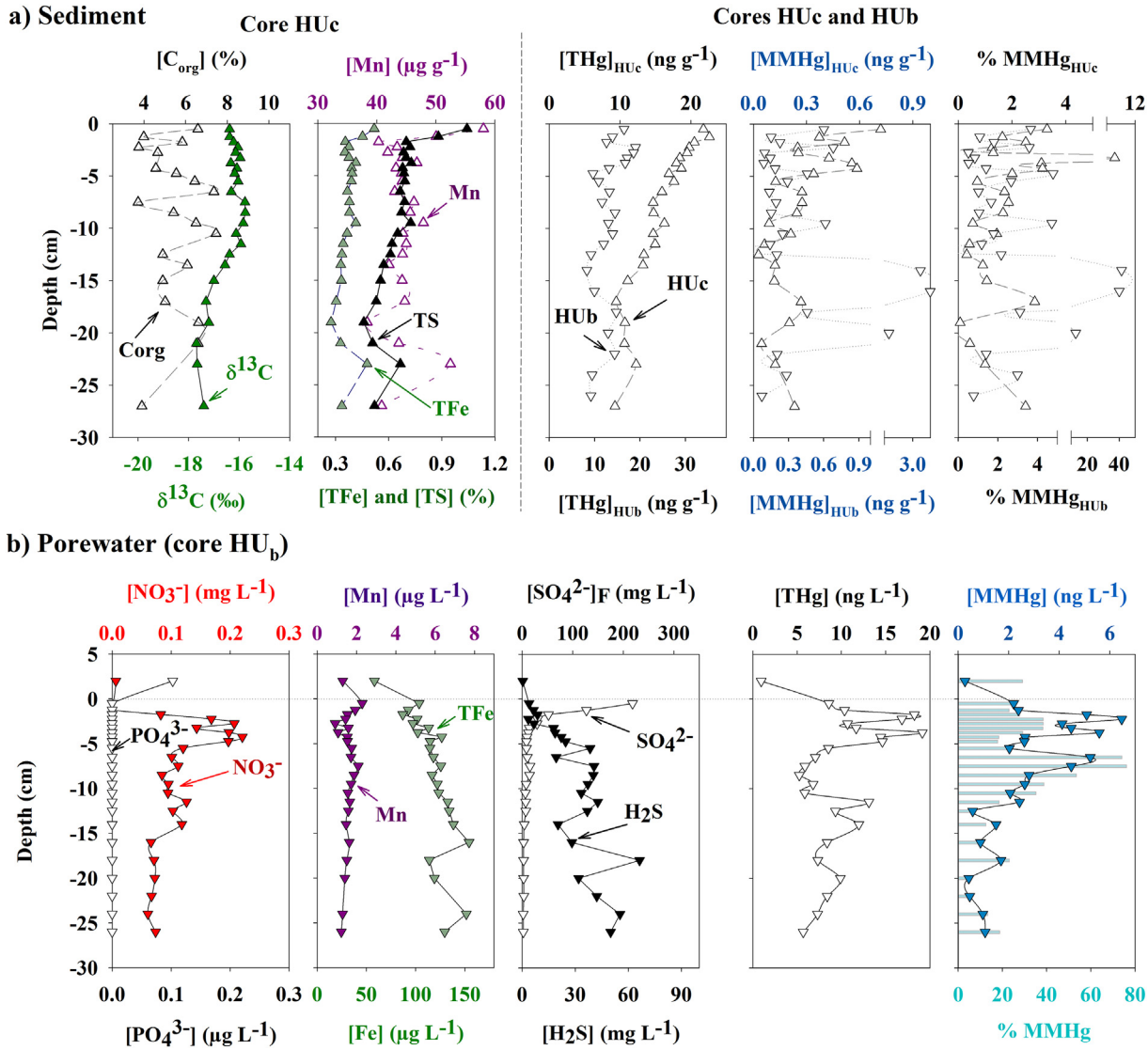

Fig. 2. Carbonate rich shallow sediment (cores HU, Huatajata). Depth concentration profiles in: a) sediment: Corg, $\delta^{13}Corg_{(VPDB)}$, Mn, TFe, TS, THg, MMHg and %MMHg and b) porewater: NO_3^-, PO_4^{3-}, Mn, Fe, SO_4^{2-}, H_2S and THg*, MMHg* and % MMHg*. All parameters are provided for the core HUc and * are from both cores HUc and HUb. Subscript c refers to sediment covered by *Characeae* (HUc) and b by epibenthic biofilms (HUb). The complete data for the porewater of cores HUc and BCc (outlet of the Cohana Bay) are presented in Fig. S3.

(Fig. S1). The density and height of the *Characeae* mats varied greatly between sites with the highest ones (60 to 80 cm) found in the shallowest areas (core BCc, 2 m depth). In this later core, the first 7 cm of sediment were weakly consolidated with high water content (Fig. S2) and many macrophytes remains. At Huatajata (HU – Fig. 1), the density and height of *Characeae* (core HUc: 10 to 40 cm above the SWI) were lower with some areas exempted of macrophytes (core HUb) and the sediment was more consolidated. In both HU cores (covered or not by *Characeae*), the ~2 cm surface sediment was mainly constituted of epibenthic biofilms where Proteobacteria, Cyanobacteria, and Bacteroidetes were reported to dominate the active microbial communities (Bouchet et al., 2018).

Total Hg concentrations in the sediment were low (THg = 18.0 ± 11.5 ng g^{-1}) for the three cores ($N = 72$) HUc, HUb and BCc (Fig. 2 for HUc and HUb profiles and Fig. S3 for BCc profile), but in the range of previously reported values for pristine Lakes (Matty and Long, 1995; Perrot et al., 2010; Wang et al., 2010). MMHg concentrations in sediment were also low (0.3 ± 0.6 ng g^{-1} for the three cores), and rarely exceeded 1 ng g^{-1} with an average percentage over THg of 3.7 ± 8.0% ($N = 48$) at Huatajata (HUb and HUc – Fig. 2) and 0.2 ± 0.1% ($N = 24$), at the outlet of Bahia Cohana (BCc – Fig. S3); the lowest value encountered in our study. Highest MMHg concentrations were found in both HU cores within the 5 first cm, peaking at the surface sediment around 0.7 ng g^{-1} and between 15 and 20 cm depth in core HUb with values up to ~4 ng g^{-1}. THg exhibited a slight and gradual decrease with depth from ~20 to 10 ng g^{-1}.

The lowest filtered THg and MMHg concentrations were found in the OW while the highest ones (THg: 8.4 ± 3.6 ng L^{-1} and MMHg: 2.4 ± 1.9 ng L^{-1} - Figs. 2b and S3) were encountered in PW within the first 5 cm that include the epibenthic biofilm layer (0–2 cm).

In this layer, percentages of MMHg reached up to >90% in HUc and BCc cores (Figs. 2 and S3). In both HUb and HUc cores these peaks were found at the onset depth of sulfate reduction (0–3 cm) where sulfates were consumed in a narrow layer (0–2 cm) and at the first peak of H_2S (5–7 cm). Below 10 cm depth in the profile, Hg(II) depicted several peaks while MMHg gradually decreased or stood on a baseline concentration.

3.1.2. Carbonate-detrital facies of the Lago Mayor

The carbonate-detrital facies covers <20% of Lago Mayor (Rodrigo and Wirrmann, 1992). The major element composition [calcium carbonate (52 ± 4%), Fe (0.2 ± 0.05%) and Mn (31 ± 9 µg g^{-1}), N = 4 -

Fig. S5] of core IS collected close to the Sun Island (Fig. 1) was similar to those of the carbonate facies of the Lago Menor. Despite these similarities, core IS (Fig. S5) had higher DBD (dry bulk density = 0.43 ± 0.06 g cm^{-3}, $N = 9$) and lower water content (64 ± 3%, N = 9) than the three carbonate facies cores collected in the Lago Menor (Fig. S1). Similarly, both THg (75 ± 26 ng g^{-1}, N = 9) and MMHg (4.9 ± 3.4 ng g^{-1}, N = 9) were higher (up to 10–20 times) than in the Lago Menor (Figs. S1 and S5). Percentages MMHg in the sediment were in the same range as for the Lago Menor standing generally below 5%.

3.2. Organo-detrital facies of the deep areas (Chua trough – Lago Menor)

The organo-detrital facies covers approx. 5% of the sediment surface area of the Lago Menor (Table S4) and is found in the deepest areas (Fig. 1). The sediment core collected in the Chua trough (CH, $N = 24$) had a high water content (93.2 ± 2.4%) and low dry bulk density (0.021 ± 0.007 g cm^{-3}). The carbonate content was low (average $CaCO_3$ = 8 ± 8%) while OM content was high (Corg = 13.7 ± 2.5%) with $\delta^{13}C$ values (−20.15 ± 1.66; Fig. 3) typical of planktonic OM (Cross et al., 2000; Baker et al., 2001; Rowe et al., 2002). Total S concentration (1.7 ± 0.2%) and major detrital elements [i.e., Al = 3.9 ± 1.1%, Fe = 2.5 ± 0.3% and Mn = 0.025 ± 0.007%] were respectively 3 and 10 times more abundant than in the carbonate sediment. Reactive Fe (Fe_{asc}) and Mn (Mn_{asc}) decreased with depth from 15 and 30% to 5% and 10% of total Fe and Mn concentrations, respectively (Fig. S1). THg concentrations (95.1 ± 11.0 ng g^{-1}) were >5 fold higher than in carbonate rich sediments (Fig. 3a). MMHg concentrations were low (0.3 ± 0.1 ng g^{-1}) with a mean percentage of THg standing at 0.3 ± 0.2%. Highest THg and MMHg concentrations were found in surface sediment (i.e., between 0 and 3 cm depth) and in the lower part of the core around 18 cm depth (Fig. 3a).

In the PW (N = 24), THg concentrations (5.8 ± 2.2 ng L^{-1}) were slightly lower than in carbonate rich sediment (8.0 ± 3.6 ng L^{-1}) and MMHg concentrations (0.94 ± 0.30 ng L^{-1}) were almost three fold lower than in HU cores (2.9 ± 2.0 ng L^{-1}) with percentages MMHg (17.4 ± 7.4%) amongst the lowest values measured in our cores. Porewater THg was rather stable around 5 ng L^{-1} in the profile but exhibited two peaks. The first was located at ~4 cm depth coinciding with the first optimum of sulfate reduction occurring in a stretcher zonation (0–10 cm) as compared to the carbonate rich sediment, and a second at ~12 cm depth below the optimum of iron reduction, maintained along the rest of the core. MMHg concentration profiles exhibited a similar pattern with 2 peaks located within the sulfate reduction zone; below the SWI (0–2 cm) and at the first optimum of H_2S concentrations

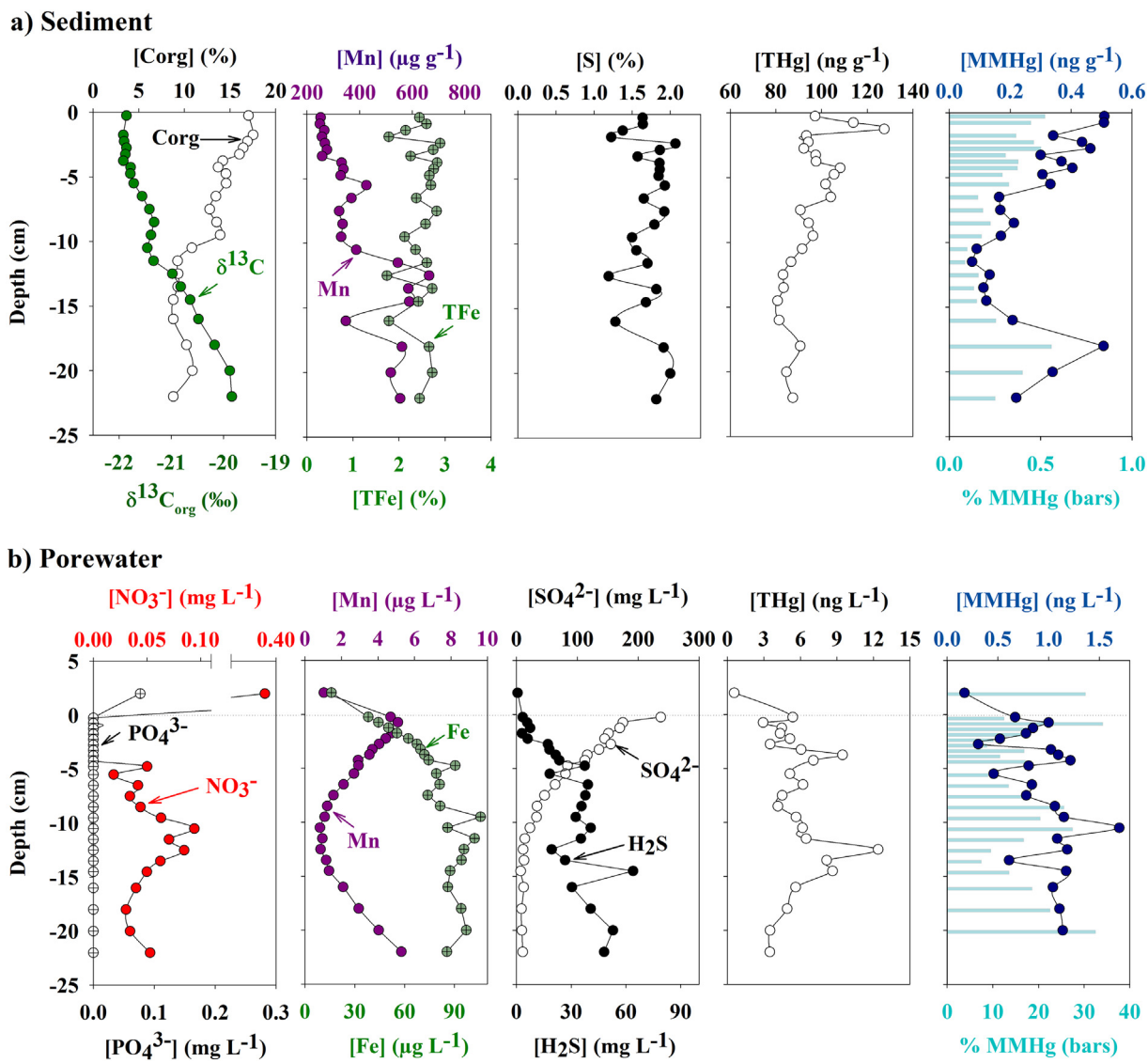

Fig. 3. Organic rich deep sediment (core CH, Chua). Depth concentration profiles in: a) sediment: Corg, $\delta^{13}Corg_{(VPDB)}$, Mn, TFe, TS and THg, MMHg and %MMHg and b) porewater: NO_3^-, PO_4^{3-}, Mn, Fe, SO_4^{2-}, H_2S, THg, MMHg and % MMHg.

(3–5 cm), and a third one at ~10 cm depth coinciding with the optimum of iron reduction (Fig. 3b). Porewater MMHg concentrations remained amongst the highest values of the profile below this peak throughout the entire Fe reduction zone except a decrease at ~ 13 cm depth while THg exhibited a gradual decrease.

3.3. Sediment facies of the littoral areas

3.3.1. Organic facies of the Lago Menor (Cohana Bay)

The organic facies is representative of very shallow (<2 m) littoral areas and covers <20% of the bottom sediments in Lago Menor (Table S4). Abundant *totora* sedges in this area provide plenty of Corg (6.7 ± 2.8%, $N = 24$) to the sediment and entrap the majority of allochthonous inputs as illustrated by high Al (5.8 ± 1.4%) and Fe (4.1 ± 0.4%) contents (N = 24, Fig. 4). This results in sedimentation rates reported amongst the highest in Lake Titicaca (Binford et al., 1992; Pourchet et al., 1994). Both Fe_{asc} (16.6 ± 2.2% Fe_{tot}, $N = 13$) and Mn_{asc} (23.6 ± 8.8% Mn_{tot}) were high in the top 10 cm and sharply dropped below to average values of 5.7 ± 1.4% Fe_{tot} and 9.6 ± 1.2% Mn_{tot} ($N = 7$), respectively (Fig. S1). Core BCt was sampled in the middle of the very shallow eutrophic Cohana Bay (Fig. 1) which receives discharges of urban effluents from El Alto city through the Katari River (Archundia et al., 2017; Molina et al., 2018). Such discharges leads to the eutrophication of the Bay (Acha et al., 2018) as illustrated by phosphate concentrations reaching ~1 μg L^{-1} in the 10 first cm in PW of core BCt (Fig. 4). This very shallow coastal sediment has been subject to various changes in water column level in the recent history of the lake (Weide et al., 2017). Such changes are illustrated in both the sediment lithology and chemistry with the presence of a compact layer starting below 15 cm depth characterized by low Corg and Mn concentrations but high Fe content below this interface (Fig. 4). δ^{13}Corg values also illustrate these changes in sedimentation and ecotopes, with the most negative δ^{13}Corg found in the top 2 cm sediment (−26.7 ± 0.5‰, $N = 4$) and the deep layer (−23.8 ± 1.1‰, $N = 6$) which are typical of the presence of emerged aquatic plants OM (i.e., totoras sedges) while in the sedimentary part between 4 and 14 cm depth, δ^{13}Corg has heavier values (−22.0 ± 0.4‰, N = 13) together with higher carbonate content (18.5 ± 5.6%) suggesting a mixed contribution of submerged macrophytes (*characeae*) and emerged (totoras) aquatic plants (Valero-Garcès et al., 1999).

In the sediment (N = 24), THg (39.8 ± 5.0 ng g^{-1}) were in the medium range of concentrations found in Lago Menor. Similar to the

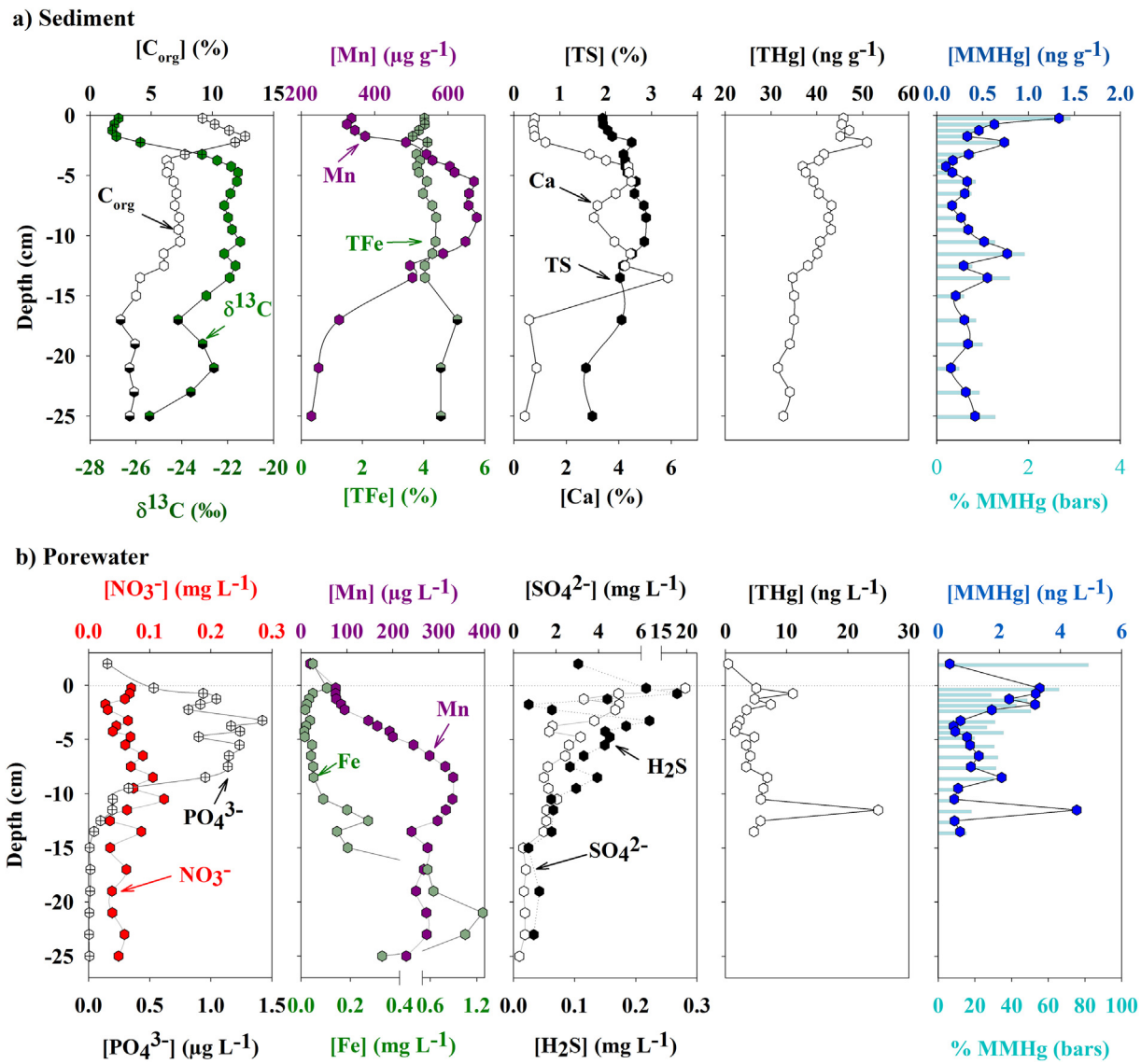

Fig. 4. Organo-detrital littoral sediment (core BCt, very shallow eutrophic Cohana Bay). Depth concentration profiles in: a) sediment: Corg, $\delta^{13}Corg_{(VPDB)}$, Mn, TFe, TS and THg, MMHg and % MMHg and b) porewater: NO_3^-, PO_4^{3-}, Mn, Fe, SO_4^{2-}, H_2S, THg, MMHg and % MMHg. Crossed symbols refer to biofilm rich surface sediment layer and semi-filled symbols to the compact layer below 15 cm deep.

organo-detrital facies, both MMHg (0.4 ± 0.3 ng g^{-1}) and % MMHg were low (1.0 ± 0.6%) and exhibited the highest concentrations in the surface layer and a slight increase (11–13 cm) above the transition with the compact layer.

In the PWs, sulfides concentrations were 2 to 3 orders of magnitude lower than in the carbonate and the organo-detrital facies and the sulfide reduction occurred as for CH within a stretched zone from the OW (H_2S = 3 mg L^{-1}) to the 15 first cm depth were sulfates were not detected. Below 12 cm depth, Fe reduction became dominant and PW Fe concentrations exhibited a sharp rise from ~0.05 to 1.05 mg L^{-1} which overwhelmed H_2S concentrations. Average THg in PW was low (4.4 ± 1.7 ng L^{-1}, $N = 18$) except two peaks up to 11 and 25 ng L^{-1} below the SWI (0–2 cm) and at 12 cm depth. PW MMHg concentrations (1.6 ± 1.2 ng L^{-1}, N = 18) were in the lowest range encountered in our dataset with the exception of two peaks found below the SWI (3.2 ng L^{-1}) and at 12 cm depth (4.5 ng L^{-1}). Highest percentages MMHg up to 60% were found in the first peak which coincided with the highest H_2S values of the profiles. Downward in the sediment, both %MMHg and concentrations remained low with the exception of a thin peak at 12 cm coinciding with the onset of the Fe reduction illustrated by the first rise of Fe in PW.

3.3.2. Detrital facies of the Lago Mayor (Escoma Bay)

The sediment of the Escoma bay (core BE, $N = 14$) originate mainly from the Rio Suchez which flows through the upstream goldmining sites of the Suches – Antaquilla placers (Herail et al., 1991). The core collected in the Bay (core BE, 24 m depth – Figs. 1 and S8) was mainly composed of clastic components originating from the riverine discharges and had low OM content (Corg <2.5%, Fig. S8) with typical $\delta^{13}C$ signatures (average −24.4 ± 0.5‰) of C_3 puna grasses (Valero-Garcès et al., 1999). THg concentrations (66.1 ± 10.4 ng g^{-1}) were in-between those of BCt and CH cores. These THg concentrations were much lower than those reported for contaminated sites from mining activities in the Altiplano (Alanoca et al., 2016b) suggesting that the great distance to the upstream goldmines had likely reduced their impact through sedimentation in the upstream alluvial plain. Percentage MMHg (1.2 ± 0.4%) in core BE sediment was low although concentrations (0.8 ± 0.3 ng g^{-1}) were amongst the highest ones in our data set (Fig. S8).

In the PW (N = 14), H_2S concentrations were as low as in the Cohana Bay core BCt while both Fe and Mn were at least 3 orders of magnitude higher in the entire profile likely due to a large detrital pool. Fe and H_2S exhibited a mirror distribution with rising Fe concentrations while H_2S decreased. Porewater THg concentrations (12.9 ± 8.6 ng L^{-1}) were in the highest range of our data and exhibited a peak up to 30 ng L^{-1} below the SWI followed by a gradual decrease with depth down to 2.7 ng L^{-1} at 12 cm depth. MMHg concentrations (1.5 ± 0.8 ng L^{-1}) and percentages (15 ± 10%) in PWs were low in the entire profiles with the exception of two thin peaks located below the SWI (3.7 ng L^{-1}) within the optimum of sulfate reduction and a second one (2.1 ng L^{-1}) at 9 cm depth within the Fe reduction coinciding with a sulfide peak (Fig. S8).

4. Discussion

4.1. OM, Fe and S control on the partitioning of Hg between sediment and porewater

THg in the sediment was found correlated with C_{org} in all cores with the exception of the carbonate rich sediments (Fig. 5). In the organic rich cores (CH and BCt), although the regression slopes were similar, their y-intercepts were at least 2 times greater for CH than for BCt, whereas the Corg depleted core BE had almost 2 times higher THg concentrations than BCt. It suggests that the abundance of C_{org} was not limiting for Hg scavenging but rather that the quality of OM (Skyllberg et al., 2000; Skyllberg, 2012) and especially its reduced sulfur content increased the ability of sediment OM to bind Hg (Hollweg et al., 2009). Hence, Hg had.

a higher affinity for allochthonous OM (BE) than for autochthonous OM (CH and BC) (Hammerschmidt et al., 2008). Amongst autochthonous OM, the fine pelagic OM (CH) was a greater Hg scavenger than OM mostly originating from emerged aquatic plants in the littoral (core BCt, Fig. S9). In addition, the positive correlation between Hg or other redox sensitive elements (Mo, Cd and U) with both authigenic Fe sulfide minerals and Corg (Figs. 4 and S6) at Chua support their scavenging onto sulfidized OM (Chappaz et al., 2008; Marnette et al., 1992; Rosenthal et al., 1995; Schaller et al., 1997) likely present as organic coating on authigenic Fe minerals (Feyte et al., 2012). Another explanation for the difference in THg concentration between cores is the different sedimentation rate which are much lower in the deep sites [0.05 to 0.1 cm yr^{-1} (Rodrigo and Wirrmann, 1992)] compared to the much shallower sites [e.g., 0.22 to 1 cm yr^{-1} (Binford et al., 1992; Pourchet et al., 1994)] where the high production of autochthonous OM and carbonates, and the trapping of allochthonous material dilutes Hg concentrations. In the carbonate rich sediment (HUc), THg was positively correlated with TS ($R = 0.93$), TFe ($R = 0.61$) and Fe_{asc} ($R = 0.81$) but not with C_{org} (Figs. 5 and S4). Hence, Hg was likely adsorbed onto authigenic Fe sulfides in this type of sediments in contrast to the organic rich ones. The positive correlation between both TFe or Fe_{asc} and TS ($R = 0.87$ and 0.93, respectively), the Fe:S molar stoichiometry (average = 0.36 ± 0.03), and the respective abundance of TFe and Feasc support a sediment composition with (i) a major pool of pyrite (FeS_2) and (ii) a minor pool of other sulfide minerals (or OM) and reactive Fe minerals (i.e., Feasc = 4.2 ± 1.2%TFe) extracted by ascorbate (Canfield et al., 1992; Hyacinthe et al., 2001). These results are in accordance with the moderate levels of AVS (12–56 μmol g-1) reported in the Lago Menor shallow surface sediments (Sarret et al., 2019).

In PWs, highest THg concentrations were encountered in the surface layers of the carbonate rich sediment core (HUb and HUc) and decreased with increasing Fe and H_2S concentrations (Fig. 5b) with depth. In addition, both PW Fe and H_2S were positively correlated suggesting the presence of filter passing colloidal FeS minerals as reported in anoxic waters and PW (Brendel and Luther, 1995; Bura-Nakic et al., 2009). In opposition, PW THg concentrations in organic rich sediments were at least 2 times lower and increased with rising filtered Fe concentration but did not exhibit any covariations with H_2S (Fig. 5) suggesting that Hg was bound to organic ligands in solution.

The calculation of partition coefficients for Hg(II) between the sediment and the PWs ($\log K_D = \log [Hg(II)_{sed}] - \log[Hg(II)_{PW}]$) corroborates the hypothesis that sediment OM content and source (or quality) controlled the partitioning of Hg(II) onto the solid phase because $\log K_D$s for Hg(II) at CH (= 4.2 ± 0.2, $N = 24$), BCt (3.9 ± 0.3, $N = 18$) and BE (3.8 ± 0.3, $N = 14$) cores were much higher than those of the 3 carbonate facies sediment cores (3.4 ± 0.3, $N = 72$). In the carbonate rich sediment, the enhanced partitioning of Hg(II) into the porewater phase can result from both the low Corg content in the sediment and the high sulfide content in PWs reported to favor Hg—S complexes in pore fluids (Drott et al., 2007; Skyllberg, 2008) and/or as Hg bound to colloidal Fe sulfides.

4.2. OM, Fe and S control on the MMHg accumulation in sediment and PW

The distribution of MMHg in sediments was found closely associated to the one of THg in HU and CH cores (Fig. 6a). In the carbonate rich sediment (HU), MMHg was found associated to authigenic Fe sulfides while in the organic rich sediment core CH, it was likely associated to sulfidized OM and authigenic Fe minerals (Fig. 6). In opposition, no correlations were found between MMHg and C_{org}, Fe or S for the two littoral cores (BCt and BE) suggesting that only specific fractions of their mixed source OM and other minerals have driven the sorption of MMHg.

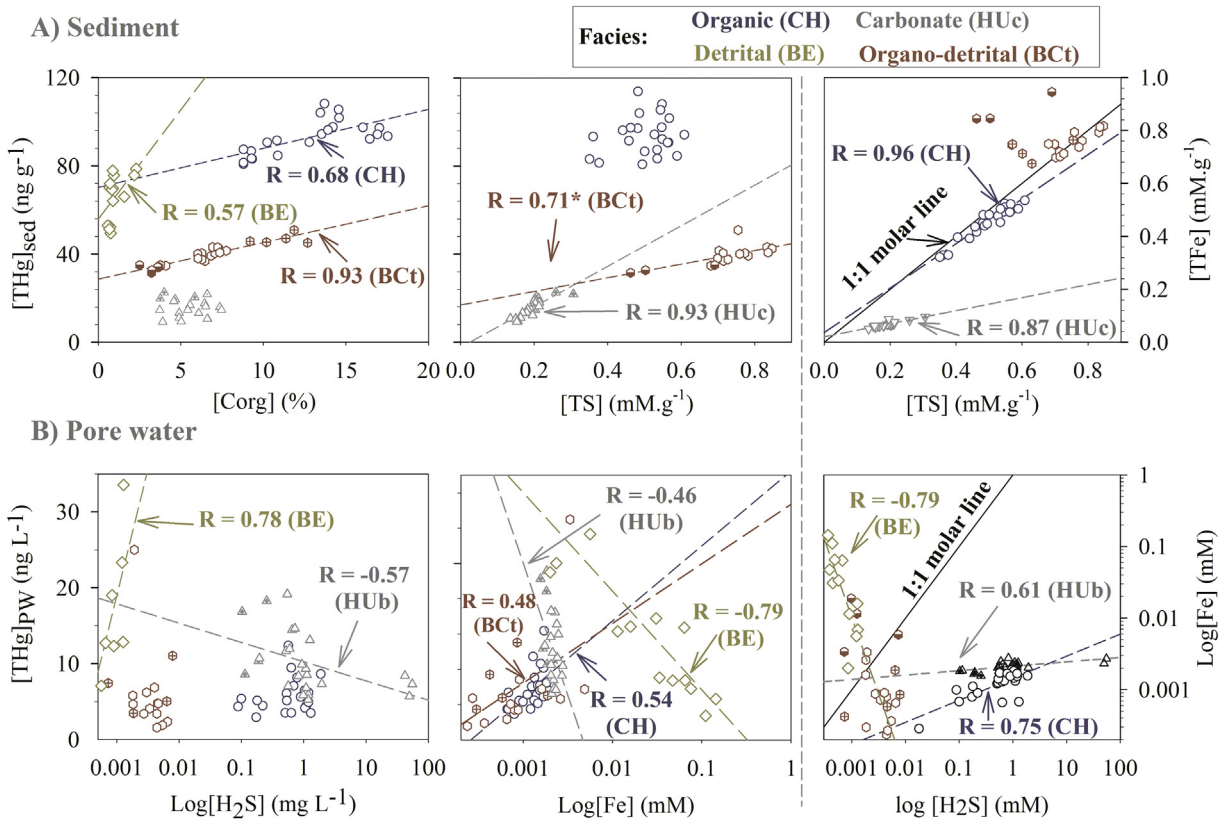

Fig. 5. Relationships between (from left to right): A) THg and Corg, THg and TS, and Ts and TFe concentrations in the sediment and B) THg and Log H_2S, THg and LogTFe, and Log H_2S and LogTFe concentrations in the porewater. Regressions are plotted only for *p* values <0.01. Colored symbols and regression lines refer to: the very shallow organo-detrital facies at Cohana Bay (red circles, core BCt), the shallow carbonate facies at Huatajata (grey triangles, core HUc), the organic-rich deep facies at Chua (dark blue circles, core CH) and the detrital facies at Escoma Bay (dark red hexagons, core BE). Crossed symbols refer to surface sediment (biofilm) and semi-filled symbols to the compact layer below 15 cm deep in core BCt. * regression performed without 0–2 cm biofilm layer in core BCt. (For interpretation of the references to colour in this figure legend, the reader is referred to the web version of this article.)

In PWs, MMHg peaks occurred in surface sediments for our entire set of cores at depth intervals where sulfates were consumed (Figs. 2–4, S3 and S8). This suggests that in subsurface sediments, MMHg production by sulfate-reducing bacteria was favored by the presence of fresh OM and low-molecular-weight (LMW) thiols that promote Hg bioavailability (Drott et al., 2007; Bouchet et al., 2018). The highest MMHg accumulation in surface HU cores was likely related to low DOM and high colloidal (Fe or Hg) sulfides and/or charged complexes, e.g. HgS_2H^- and HgS_2^{2-} that favored biomethylating (Drott et al., 2013) compared to the other facies where high DOM have likely restricted Hg(II) availability for methylators (Barkay et al., 1997).

Deeper in the profiles, the differences in MMHg concentrations and percentage patterns between cores can be related to the decrease of LMW ligand with depth (Vairavamurthy et al., 1997) and to their respective amounts of H_2S and Fe in PWs. Our set of cores can be divided in three groups with PWs H_2S > Fe in the entire HU and CH profiles, H_2S ≥ Fe in core BCt and H_2S ≤ Fe in core BE (Fig. 5). In CH and BCt cores, MMHg in PWs did not show any significant relationship with H_2S in contrast to cores HU and BE although the highest MMHg values were found at different H_2S concentrations in these laters (Fig. 6). Thus, we find no support for a general trend in decreasing concentration of accumulated MMHg at a certain concentration of sulfide, owing to the decreasing of dissolved neutral Hg sulfides concentrations, as previously proposed (Benoit et al., 1999).

In the PWs of the carbonate rich sediment (HU), the gradual decrease with depth of both Hg(II) and MMHg with increasing H_2S and Fe concentration (Fig. 6) suggests that Hg (II) became unavailable for methylating organisms (Liu et al., 2008) as it likely precipitated as HgS or was adsorbed onto neoformed sulfides (Slowey and Brown, 2007). In core BE, although H_2S and Fe levels were at least respectively 3 orders of magnitude lower and higher than those of HUb, similar trend was found with an in depth decrease in THg with increasing Fe concentration illustrating that the abundance of Hg species in PW was controlled by sulfides until iron reduction became dominant favoring the scavenging of Hg species onto precipitated authigenic minerals as reported in various freshwaters (Feyte et al., 2010; Feyte et al., 2012; Hellal et al., 2015) and marine sediments (Cossa et al., 1996; Gobeil et al., 1999; Guédron et al., 2012). However, it must be considered that the decline with depth of PWs and sediment MMHg concentration may result from increasing demethylation (Rydberg et al., 2008).

In the PWs of the organo-detrital sediment (core CH), MMHg concentrations and percentages were almost 3 times lower than in the carbonate facies in spite of a similar range of H_2S concentration. The same was found for the detrital core BCt although H_2S levels were at least 3 orders of magnitude lower. In addition, PW THg in both cores were amongst the lowest values suggesting that H_2S was not the unique driver of Hg(II) availability for biomethylation. Again, sediment OM have likely enhanced the partitioning of Hg species onto the solid phase or demethylation was higher in these cores.

Below ~10 cm depth, highest MMHg concentrations (core CH – Fig. 3) or peaks (cores BCt and BE – Figs. 4 and S8) were found at the onset or within the iron reduction zone. Hence, in these 3 cores enriched in Fe, IRB likely took over SRB for methylation independently of the H_2S level when iron overwhelmed sulfate reduction (Fig. 5).

Finally, as for Hg(II), the plot of MMHg log K_{Ds} values against C_{org} (Fig. 6) corroborates the hypothesis that sediment OM quality controls the partitioning of MMHg between sediment and PWs because lowest log K_{D}s were found in the OM depleted carbonate cores (average log K_{DMMHg} for HUc, HUb and BCc = 1.9 ± 0.6, $N = 72$) compared to the organic rich sediment facies (log K_{DMMHg} = 2.4 ± 0.4 and 2.5 ± 0.3 for CH

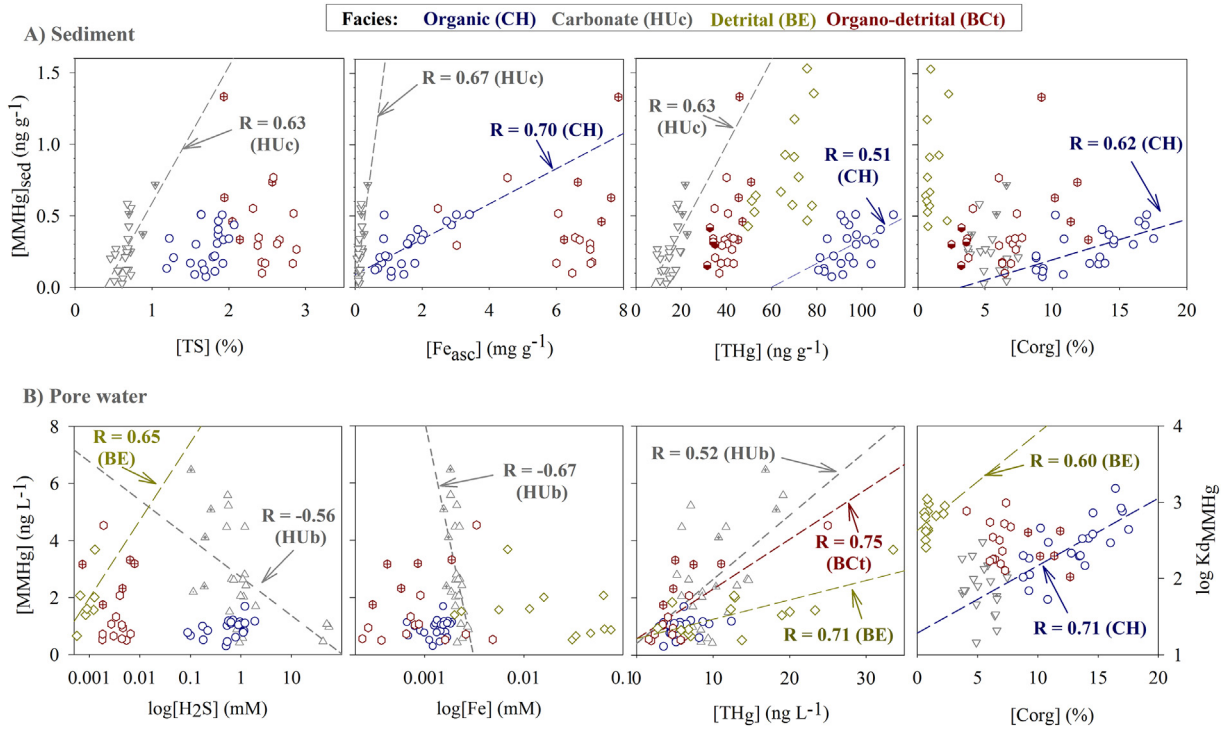

Fig. 6. Relationships between (from left to right): A) MMHg and TS, MMHg and Fe extracted with ascorbate (Fe_{asc}), MMHg and THg, and MMHg and Corg concentrations in the sediment and B) MMHg and Log H_2S, MMHg and LogTFe, MMHg and THg concentrations in porewater. The bottom right panel shows the relationship between log $K_{d\ MMHg}$ and Corg. Regressions are plotted only for p values <0.01. Colored symbols and regression lines refer to: the very shallow organo-detrital facies at Cohana Bay (red circles, core BCt), the shallow carbonate facies at Huatajata (grey triangles, core HUc), the organic-rich deep facies at Chua (dark blue circles, core CH) and the detrital facies at Escoma Bay (dark red hexagons, core BE). Crossed symbols refer to surface sediment (biofilm) and semi-filled symbols to the compact layer below 15 cm deep in core BCt. (For interpretation of the references to colour in this figure legend, the reader is referred to the web version of this article.)

($N = 24$) and BCt ($N = 18$), respectively). Again, the highest values were found in the OM depleted core BE (log $K_{DMMHg} = 2.8 \pm 0.2$, $N = 14$) where the terrestrial Corg has likely the highest binding capacity in comparison to the other types of OM.

4.3. Estimation of Hg(II) and MMHg diffusive fluxes toward the water column

In all cores, the drop in Fe and Mn concentrations above the SWI indicates the existence of a strong redox front at the SWI where reduced Fe and Mn (diffusing from the PW) were back oxidized and precipitated as reactive Fe- and Mn-oxides [i.e., Fe_{asc} and Mn_{asc}, Fig. S1 (Davison, 1993; Boudreau, 1999)] likely trapping the Hg released during OM mineralization (Figs. 2 to 4). Hence, only a fraction of Hg from the PWs is transferred into the upper water column depending on (i) the steepness and thickness of the redox stratification around the SWI (Berner, 1980), (ii) the adsorption of Hg by biota [e.g., biofilm and periphyton (Lanza et al., 2017; Bouchet et al., 2018)], (iii) the diffusivity of Hg binding ligands [e.g., macromolecules and colloids (Skyllberg, 2008; Guédron et al., 2016; Bouchet et al., 2018)], and (iv) the bioirrigation or physical advection (Point et al., 2007; Cardoso et al., 2008; Guédron et al., 2012). Although we could not provide all these parameters, the high resolution gradient profiles obtained at the SWI in the sediment cores allow us calculating a first estimate of the Hg diffusive fluxes using the first Fick's law (see Section 2.5 for calculation details) from the different sediment facies. These calculations were only performed for the Lago Menor because of the limited number of cores in Lago Mayor.

The obtained MMHg diffusive fluxes (Jsed) were always positive (efflux from the sediment into the overlying water column) rising from the deep (13 ± 2 ng·m^{-2}·d^{-1}), to the littoral (53 ± 8 ng·m^{-2}·d^{-1}) organic facies and to the shallow carbonate facies (104 ± 16 ng·m^{-2}·d^{-1} – Table 1 and S.I.6). These values are within the highest values (from 1 to 270 ng·m^{-2}·d^{-1}) reported for contaminated freshwater areas (Gill et al., 1999; Choe et al., 2004; Guédron et al., 2012). As expected, sediments of the carbonate facies which cover almost 75% of the Lago Menor (Table S4) were found the greatest contributor of MMHg to the water column because they combine the lowest logK_D and the highest MMHg concentration gradients between PW and OW. The estimated daily MMHg diffusive fluxes reported to the lake bottom surface area of each of the 3 sediment facies, were respectively; 0.75 g·d^{-1} for the organic-detrital facies, 15 g·d^{-1} for the organic facies and 102 g·d^{-1} for the carbonate facies and a total daily flux of 118 g·d^{-1} at the scale of Lago Menor (Table 1).

Because large diel and seasonal changes in MMHg concentrations were reported in surface water due to extreme (de)methylation oscillations during diurnal biogeochemical gradients (Alanoca et al., 2016a; Bouchet et al., 2018), we calculated diel and seasonal diffusive fluxes by comparing fluxes obtained with extruded cores to fluxes obtained with Rhizon (micro-needle sampler) collected by scuba divers during a ~2 h sampling period at various periods of the day (Fig. 7). The Rhizon experiments could only be conducted in very shallow (BCc) and shallow (HUc and HUb) areas due to diving constrains. Obtained diffusive fluxes from Rhizon samplers and extruded cores were of similar ranges and consistent within studied periods (Fig. 7). During the late wet season, MMHg fluxes overwhelmed those of Hg(II) strikingly showing that diffusion of THg toward the water column was dominantly composed of MMHg (Fig. 7a).

Hg(II) diffusive fluxes were higher in the early morning and no significant difference was found between sediment covered by *epi*benthic biofilms or *Characeae*. For MMHg, fluxes showed a decreasing trend from the early morning to the afternoon for sediment covered by *Characeae* while they remained almost constant for sediment covered by epibenthic biofilms. During the late dry season, Hg(II) diffusive fluxes were generally higher than for the late wet season with the highest fluxes found at noon for all sites. However, the lack of data for the early morning period doesn't allow concluding. MMHg fluxes were

Table 1
Mean diffusive fluxes (Jsed) calculated for Hg(II) and MMHg from the difference between surface PW (0 to 1 cm) and OW for the 3 main sediment facies of Lago Menor and reported to their respective surface area (two left columns).

Sediment facies [depth range]	Cores	Surface (km^2)	Volume (km^3)	Jsed Hg(II) ($ng \cdot m^{-2} \cdot d^{-1}$)	Jsed MMHg ($ng \cdot m^{-2} \cdot d^{-1}$)	Jsed Hg (II) ($g \cdot d^{-1}$)	Jsed MMHg ($g \cdot d^{-1}$)
Organic [0–2 m]	BCt	267.8	2.3	15.1	55.4	4.0	14.8
Carbonate [2–20 m]	HUc Hub BCc	983.9	7.6	57.2	104.0	56.3	102.3
Organo detrital [20–40 m]	CH	57.0	0.7	9.7	13.2	0.6	0.75
Total		1308.7	10.6			60.9	117.9

only measured at noon during the dry season but were amongst the lowest values recorded for the two seasons. Although the data set is not exhaustive, our temporal set of data suggests that during the wet season, carbonate sediment covered by *Characeae* are the main source of MMHg for the water column with higher fluxes found in the early morning.

OW used for these calculations were collected within the 50 cm above the sediment and had similar narrow MMHg concentrations range (average = 0.08 ± 0.04 $ng \cdot L^{-1}$, $N = 40$) for the three sites) to those reported in the water column [0.11 ± 0.06 $ng \cdot L^{-1}$ (Guédron et al., 2017)] but were 4 times lower than the siphoned OW (0–5 cm) recovered in cores (average MMHg = 0.33 ± 0.07 $ng \cdot L^{-1}$ for the three sites, $N = 5$). Such difference reflects the stratification in the epibenthic layers and the strong gradient between epibenthic and surface water from which resulted an overestimation of the fluxes obtained with rhizons. This points out the importance of the benthic/epibenthic stratification in the water column above the SWI as a modulating factor on the use of calculated diffusive flux to estimate representative flux budget. Indeed, higher fluxes found in the early morning could be explained by a shallower redox front (e.g., into the *Characeae* mat) during the night resulting from the aquatic ecotopes respiration which could favor upward Hg diffusion consistently with reported higher night-time benthic chambers in the Lavaca Bay (Gill et al., 1999). In contrast, the macrophytes photosynthesis during the day may favor the water column oxygenation and the scavenging of MMHg in the Fe redox loop and onto submerged macrophyte's periphyton or benthic biofilms. Moreover, the wind driven vertical mixing of the water column during the afternoons or storm events (Dejoux, 1992) may results in two opposite processes with the flushing of porewater to the water column by physical advection (Huettel and Webster, 2001; Guédron et al., 2012; Bouchet et al., 2013) and the shifting and thinning the diffusive boundary layer downwards in the sediment (Kelly-Gerreyn et al., 2005). This later would result in a higher scavenging of dissolved or colloidal Hg species onto the surface sediment as illustrated by peaks found in surface cores (Figs. 2 and 4). However, the changes in diffusive fluxes also greatly depended on the MMHg concentration in PW which changed over time (Fig. 7). Hence, both the higher MMHg production during the night with an upward shift of the stratification likely enhanced these MMHg effluxes to the water on this period. Finally, as bioirrigation effect is not taken into account in the diffusive flux calculations, our

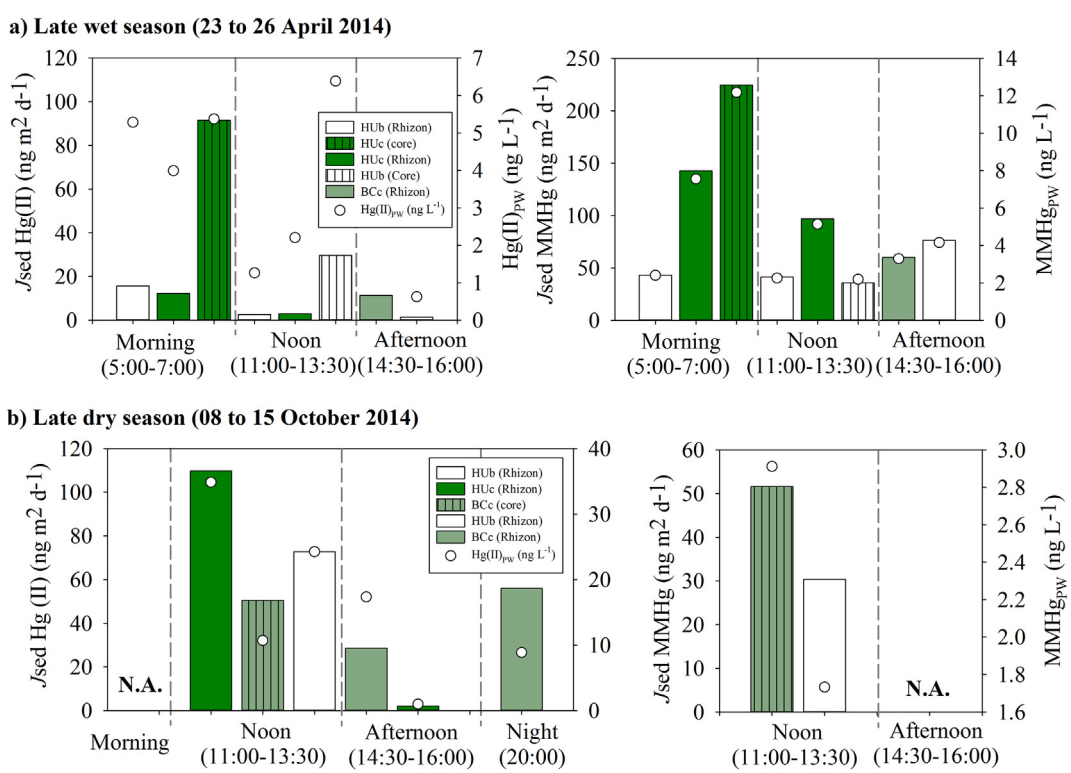

Fig. 7. Bar chart presentation of diffusive fluxes (Jsed) for Hg(II) and MMHg calculated between the first centimeter of sediment porewater and overlying (core) or surface water for shallow carbonate facies sediment (HUc and HUb: Huatajata; and BCc: Cohana Bay) at various periods of the day and for the late wet (a) and dry (b) season. Bars with vertical lines correspond to Jsed obtained from sediment cores, the others are from Rhizon (micro-needle) samplers. White symbols give the concentration of Hg(II) and MMHg in the porewater (scales on the right side of the plots).

results may underestimated total sediment-water fluxes as shown in various studies (Choe et al., 2004; Point et al., 2007; Hammerschmidt and Fitzgerald, 2008; Benoit et al., 2009).

In the water column, the accumulation of MMHg results from the equilibrium between the production of MMHg from various sources (i.e., the sediment, the benthic biota, the water column and the atmosphere), and its demethylation or its recycling (adsorption and settling) onto suspended particles and benthic biota (adsorption and absorption). The daily contribution of rain (0.003 pg MMHg.L^{-1}.d^{-1}) to the surface water of the Lago Menor can be neglected considering an average MMHg concentration in rain [0.11 ± 0.06 ng·L^{-1} o] and an annual precipitation value of 758 mm.yr^{-1} over the Lago Menor (surface = 1308.7 km^2, volume = 10.6 km^3, Table S4). The same calculation for the sediment gives a daily dissolved MMHg efflux to the water column of 11 pg.L^{-1}.d^{-1} which represents a daily input of approximately 40% to the MMHg stock in the water column of the Lago Menor [average MMHg concentration of 27 pg.L^{-1} (Guédron et al., 2017)]. In addition, we recently reported that methylation was almost negligible in the surface water while the net daily demethylation rates ranged between 10 and 40% for both the dry and wet season (Amouroux et al., 2015). Hence, these findings suggest that sediment and the (epi)benthic biota (Bouchet et al., 2018) are the main sources of MMHg for the water column in Lake Titicaca and that diffused and advected MMHg is counterbalanced by biological and photochemical demethylation, and bio-uptake in the water column.

5. Conclusions

This high-resolution early diagenesis study of the Lake Titicaca surface sediments showed evidence that MMHg accumulation in porewater and sediment was driven by the respective interplay between sources/quality of OM and bacterial mediated redox transformation of Fe and S. Our main conclusions are:

(i) highest MMHg accumulation in PW were found in surface sediment of the carbonate rich facies mostly driven by sulfate reducing organisms.
(ii) the abundance and quality of the sediment organic matter restricted MMHg accumulation in PW resulting from higher partitioning of Hg onto sediment's sulfidized OM and potentially to higher DOM in PW that was limiting for methylation. Terrestrial OM was identified as the greater scavenger of Hg in sediments compared to autochthonous OM.
(iii) the calculation of diffusive fluxes highlighted that the carbonate facies was the major contributor of MMHg for surface water with the highest fluxes occurring during the early morning when the redoxicline is suggestively located above the SWI. A preliminary mass balance on the entire Lago Menor, suggests that surface sediment could contribute to more than one third of the MMHg accumulated in the water column.
(iv) to better assess the contribution of MMHg effluxes to the water column, advective mixing (e.g., shear stress and bioirrigation) needs to be investigated to get a complete and accurate picture of Hg fluxes dynamics at the daily scale. In addition, the recent enhancement of water column eutrophication can be a major issue for such MMHg effluxes because lasting sub to anoxic conditions in the water column would likely favor both the production and the benthic fluxes toward the water column.

CRediT authorship contribution statement

S. Guédron: Funding acquisition, Conceptualization, Methodology, Investigation, Formal analysis, Writing - review & editing. **S. Audry:** Conceptualization, Methodology, Investigation, Writing - review & editing. **D. Acha:** Investigation, Writing - review & editing. **S. Bouchet:** Investigation, Writing - review & editing. **D. Point:** Investigation, Writing - review & editing, Funding acquisition. **T. Condom:** Investigation, Data curation. **C. Heredia:** Investigation. **S. Campillo:** Investigation, Resources. **A. Baya:** Investigation. **A. Groleau:** Investigation. **E. Amice:** Investigation. **D. Amouroux:** Supervision, Project administration, Funding acquisition, Writing - review & editing.

Declaration of competing interest

The authors declare that they have no known competing financial interests or personal relationships that could have appeared to influence the work reported in this paper.

Acknowledgments

This work is a contribution to the LA PACHAMAMA project (ANR CESA program, N° ANR-13-CESA-0015-01, PI: D. Amouroux: david.amouroux@univ-pau.fr) and TRACISOMER supported by a grant from Labex OSUG@2020 (PI: S. Guédron: stephane.guedron@ird.fr). S. Guédron (ISTerre/IRD/UGA) is part of Labex OSUG@2020 (Investissements d'avenir – ANR10 LABX56).

We wish to thank, J. Gardon, A. Terrazas, C. González, N. Clavijo, L. Salvatierra, R. Rios, J.C. Salinas, A. Castillo, M. Claure, J. Tapia (IRD Bolivia), Israel Quino-Lima, Jimena Yupanqui, Oswaldo Ramos and Jorge Quintanilla (IIQ – UMSA, Bolivia) and the Catari Family (Don Ramon, Don Maximo, Don Eric, Don Ruben and Dona Maria) for their help and assistance during the field campaigns and laboratory work.

Appendix A. Supplementary data

Supplementary data to this article can be found online at https://doi.org/10.1016/j.scitotenv.2020.138088. The complete dataset to this article can be found online at: http://dx.doi.org/10.17632/cdd3jndhf3.1

References

Acha, D., Iniguez, V., Roulet, M., Guimaraes, J.R.D., Luna, R., Alanoca, L., et al., 2005. Sulfate-reducing bacteria in floating macrophyte rhizospheres from an Amazonian Floodplain Lake in Bolivia and their association with Hg methylation. Appl. Environ. Microbiol. 71, 7531–7535.

Acha, D., Guédron, S., Amouroux, D., Point, D., Lazarro, X., Fernandez, P., et al., 2018. Algal bloom exacerbates hydrogen sulfide and methylmercury contamination in the emblematic high-altitude Lake Titicaca. Geosciences 8, 438.

Alanoca, L., Amouroux, D., Monperrus, M., Tessier, E., Goni, M., Guyoneaud, R., et al., 2016a. Diurnal variability and biogeochemical reactivity of mercury species in an extreme high altitude lake ecosystem of the Bolivian Altiplano. Environ. Scie. Pollut. Res. 23, 6919–6933.

Alanoca, L., Guédron, S., Amouroux, D., Audry, S., Monperrus, M., Tessier, M., et al., 2016b. Synergistic effects of mining and urban effluents on the level and distribution of methylmercury in a shallow aquatic ecosystem of the Bolivian Altiplano. Environmental Science: Processes & Impacts 18, 1550–1560.

Amouroux, D., Point, D., Guédron, S., Acha, D., Lazzaro, X., Chauvaud, L., et al., 2015. In situ exploration of processes controlling Hg biogeochemistry in Lake Titicaca hydrosystem (Bolivian Altiplano). 12th International Conference on Mercury as a Global Pollutant. vol. 1, p. 127 Jeju Korea.

Anschutz, P., Br, Sundby, Lefrancois, L., Luther, G.W., Mucci, A., 2000. Interactions between metal oxides and species of nitrogen and iodine in bioturbated marine sediments. Geochim. Cosmochim. Acta 64, 2751–2763.

Archundia, D., Duwig, C., Spadini, L., Uzu, G., Guédron, S., Morel, M.C., et al., 2017. How uncontrolled urban expansion increases the contamination of the Titicaca Lake Basin (El Alto, La Paz, Bolivia). Water Air Soil Pollut. 228, 44.

Baker, P.A., Seltzer, G.O., Fritz, S.C., Dunbar, R.B., Grove, M.J., Tapia, P.M., et al., 2001. The history of south American tropical precipitation for the past 25,000 years. Science 291, 640–643.

Balslev-Clausen, D., Dahl, T.W., Saad, N., Rosing, M.T., 2013. Precise and accurate $\delta^{13}C$ analysis of rock samples using flash combustion-cavity ring down laser spectroscopy. J. Anal. At. Spectrom. 28, 516–523.

Barkay, T., Gillman, M., Turner, R., 1997. Effects of dissolved organic carbon and salinity on bioavailability of mercury. Appl. Environ. Microbiol. 63, 4267–4271.

Benoit, J., Gilmour, C., Mason, R., Heyes, A., 1999. Sulfide controls on mercury speciation and bioavailability to methylating bacteria in sediment pore waters. Environ. Sci. Technol. 33, 951–957.

Benoit, J.M., Shull, D.H., Harvey, R.M., Beal, S.A., 2009. Effect of bioirrigation on sediment - water exchange of methylmercury in Boston Harbor, Massachusetts. Environmental science & technology 43, 3669–3674.

Berner, R.A., 1980. Early Diagenesis. Princeton University press, Princeton.

Binford, M.W., Brenner, M., Engstrom, D.R., 1992. Temporal Sedimentation Patterns in the Nearshore Littoral of Lago Huinaimarca. Lake Titicaca, a Synthesis of Limnological Knowledge. Kluwer Academic Publishers, Norwell, MA, pp. 29–39.

Bloom, N.S., Fitzgerald, W.F., 1988. Determination of volatile mercury species at the picogram level by low-temperature gas chromatography with cold-vapor atomic fluorescence detection. Anal. Chim. Acta 208, 151–161.

Bouchet, S., Amouroux, D., Rodriguez-Gonzalez, P., Tessier, E., Monperrus, M., Thouzeau, G., et al., 2013. MMHg production and export from intertidal sediments to the water column of a tidal lagoon (Arcachon Bay, France). Biogeochemistry 114, 341–358.

Bouchet, S., Goni-Urriza, M., Monperrus, M., Guyoneaud, R., Fernandez, P., Heredia, C., et al., 2018. Linking microbial activities and low molecular weight thiols to Hg methylation in biofilms and periphyton from high altitude tropical lakes (Bolivian altiplano). Environmental science & technology 52, 9758–9767.

Boudreau, B.P., 1996. The diffusive tortuosity of fine-grained unlithified sediments. Geochim. Cosmochim. Acta 60, 3139–3142.

Boulange, B., Vargas, C., Rodrigo, L.A., 1981. La sédimentation actuelle dans le lac Titicaca. Revue d'Hydrobiologie Tropicale 14, 299–309.

Boudreau, B.P., 1999. Metals and models: Diagenic modelling in freshwater lacustrine sediments. J. Paleolimnol. 22, 227–251.

Brendel, P.J., Luther III, G.W., 1995. Development of a gold amalgam voltammetric microelectrode for the determination of dissolved Fe, Mn, O_2, and S(-II) in porewaters of marine and freshwater sediments. Environmental science & technology 29, 751–761.

Bura-Nakic, E., Viollier, E., Jézéquel, D., Thiam, A., Ciglenecki, I., 2009. Reduced sulfur and iron species in anoxic water column of meromictic crater Lake Pavin (Massif Central, France). Chem. Geol. 266, 311–317.

Canfield, D.E., Raiswell, R., Bottrell, S.H., 1992. The reactivity of sedimentary iron minerals toward sulfide. Am. J. Sci. 292, 659–683.

Cardoso, P.G., Lillebø, A.I., Lopes, C.B., Pereira, E., Duarte, A.C., Pardal, M.A., 2008. Influence of bioturbation by Hediste diversicolor on mercury fluxes from estuarine sediments: a mesocosms laboratory experiment. Mar. Pollut. Bull. 56, 325–334.

Chappaz, A., Gobeil, C., Tessier, A., 2008. Geochemical and anthropogenic enrichments of Mo in sediments from perennially oxic and seasonally anoxic lakes in Eastern Canada. Geochim. Cosmochim. Acta 72, 170–184.

Choe, K.Y., Gill, G.A., Lehman, R.D., Han, S., Heim, W.A., Coale, K.H., 2004. Sediment - water exchange of total mercury and monomethyl mercury in the San Francisco Bay - Delta. Limnol. Oceanogr. 49, 1512–1527.

Collot, D., Koriyama, F., Garcia, E., 1983. Répartitions, biomasses et productions des macrophytes du Lac titicaca. Rev. Hydrobiol. trop. 16, 241–261.

Comision Mixta Peruana Boliviana, 1977. Lago Titicaca (Lago Menor) Laguna Huiñaimarca. Direccion de Hidrografia y Navegacion de la Marina.

Cossa, D., Coquery, M., Gobeil, C., Martin, J., 1996. Mercury fluxes at the ocean margins. In: Baeyens, W. (Ed.), Global and Regional Mercury Cycles: Sources, Fluxes and Mass Balances, pp. 229–247.

Cossa, D., Averty, B., Pirrone, N., 2009. The origin of methylmercury in open Mediterranean waters. Limnol. Oceanogr. 54, 837–844.

Cross, S.L., Baker, P.A., Seltzer, G.O., Fritz, S.C., Dunbar, R.B., 2000. A new estimate of the Holocene lowstand level of Lake Titicaca, central Andes, and implications for tropical palaeohydrology. The Holocene 10, 21–32.

Davison, W., 1993. Iron and manganese in lakes. Earth Sci. Rev. 34, 119–163.

De Lange, G.J., 1986. Early diagenetic reactions in interbedded pelagic and turbiditic sediments in the Nares Abyssal Plain (western North Atlantic): consequences for the composition of sediment and interstitial water. Geochim. Cosmochim. Acta 50, 2543–2561.

Dejoux, C., 1992. Lake Titicaca: A Synthesis of Limnological Knowledge. vol 68. Kluwer Academic, Dordrecht (NLD): Boston.

Dejoux, C., 1993. Benthic invertebrates of some saline lakes of the Sud Lipez region, Bolivia. Hydrobiologia 267, 257–267.

Drott, A., Lambertsson, L., Bjorn, E., Skyllberg, U., 2007. Importance of dissolved neutral mercury sulfides for methyl mercury production in contaminated sediments. Environ. Sci. Technol. 41, 2270–2276.

Drott, A., Björn, E., Bouchet, S., Skyllberg, U., 2013. Refining thermodynamic constants for mercury(II)-sulfides in equilibrium with metacinnabar at sub-micromolar aqueous sulfide concentrations. Environmental science & technology 47, 4197–4203.

Feyte, S., Tessier, A., Gobeil, C., Cossa, D., 2010. In situ adsorption of mercury, methylmercury and other elements by iron oxyhydroxides and organic matter in lake sediments. Appl. Geochem. 25, 984–995.

Feyte, Sp, Gobeil, C., Tessier, A., Cossa, D., 2012. Mercury dynamics in lake sediments. Geochim. Cosmochim. Acta 82, 92–112.

Fitzgerald, W.F., Lamborg, C.H., Turekian, H.D., Holland, K.K., 2014. 11.4 - Geochemistry of mercury in the environment. Treatise on Geochemistry, Second edition Elsevier, Oxford, pp. 91–129.

Froelich, P.N., Klinhammer, G.P., Bender, M.L., Luedtke, N.A., Heath, G.R., Cullen, D., et al., 1979. Early oxidation of organic matter in pelagic sediments of the eastern equatorial Atlantic: suboxic diagenesis. Geochemica et cosmochemica Acta 43, 1075–1090.

García Bravo, A., Cosio, C., Chevalley, P.-A., Zopfi, J., Amouroux, D., Spangenberg, J., et al., 2014. Extremely elevated methyl mercury levels in water, sediment and organisms in a Romanian reservoir affected by release of mercury from a chlor-alkali plant. Water Res. 49, 391–405.

Garcia Bravo, A., Bouchet, S., Guédron, S., Amouroux, D., Dominik, J., Zopfi, J., 2015. High methylmercury production under iron-reducing conditions in sediments impacted by sewage treatment plant discharges. Water Res. 80, 245–255.

Gill, G.A., Bloom, N.S., Cappellino, S., Driscoll, C.T., Dobbs, C., McShea, L., et al., 1999. Sediment-water fluxes of mercury in Lavaca Bay, Texas. Environ. Sci. Technol. 33, 663–669.

Gimbert, F., Geffard, A., Guédron, S., Dominik, J., Ferrari, B.J.D., 2016. Mercury tissue residue approach in Chironomus riparius: Involvement of toxicokinetics and comparison of subcellular fractionation methods. Aquat. Toxicol. 171, 1–8.

Gobeil, C., Macdonald, R.W., Smith, J.N., 1999. Mercury profiles in sediments of the Arctic Ocean Basins. Environmental science & technology 33, 4194–4198.

Guédron, S., Grimaldi, C., Chauvel, C., Spadini, C., Grimaldi, M., 2006. Weathering versus atmospheric contributions to mercury concentrations in French Guiana soils. Appl. Geochem. 21, 2010–2022.

Guédron, S., Grangeon, S., Lanson, B., Grimaldi, M., 2009. Mercury speciation in a tropical soil association; consequence of gold mining on Hg distribution in French Guiana. Geoderma 153, 331–346.

Guédron, S., Grimaldi, M., Grimaldi, C., Cossa, D., Tisserand, D., Charlet, L., 2011. Amazonian former gold mined soils as a source of methylmercury: evidence from a small scale watershed in French Guiana. Wat. Res. 45, 2659–2669.

Guédron, S., Huguet, L., Vignati, D.A.L., Liu, B., Gimbert, F., Ferrari, B.J.D., et al., 2012. Tidal cycling of mercury and methylmercury between sediments and water column in the Venice lagoon (Italy). Mar. Chem. 130-131, 1–11.

Guédron, S., Duwig, C., Prado, B.L., Point, D., Flores, M.G., Siebe, C., 2014. (Methyl) mercury, arsenic, and lead contamination of the world's largest wastewater irrigation system: the Mezquital Valley (Hidalgo State-Mexico). Water Air and Soil Pollution 225, 1–19.

Guédron, S., Devin, S., Vignati, D.A.L., 2016. Total and methylmercury partitioning between colloids and true solution: from case studies in sediment overlying and porewaters to a generalized model. Environ. Toxicol. Chem. 35, 330–339.

Guédron, S., Point, D., Acha, D., Bouchet, S., Baya, P.A., Molina, C.I., et al., 2017. Mercury contamination level and speciation inventory in the hydrosystem of Lake Titicaca: current status and future trends. Environ. Pollut. 231, 262–270.

Guédron, S., Ledru, M.P., Escobar-Torrez, K., Develle, A.L., Brisset, E., 2018. Enhanced mercury deposition by Amazonian orographic precipitation: evidence from high-elevation Holocene records of the Lake Titicaca region (Bolivia). Palaeogeogr. Palaeoclimatol. Palaeoecol. 511, 577–587.

Guédron, S., Tolu, J., Brisset, E., Sabatier, P., Perrot, V., Bouchet, S., et al., 2019. Late Holocene volcanic and anthropogenic mercury deposition in the western Central Andes (Lake Chungará, Chile). Sci. Total Environ. 662, 903–914.

Hamelin, S., Amyot, M., Barkay, T., Wang, Y., Planas, D., 2014. Methanogens: principal methylators of mercury in lake periphyton. Environmental science & technology 45, 7693–7700.

Hammerschmidt, C.R., Fitzgerald, W.F., 2004. Geochemical controls on the production and distribution of methylmercury in near-shore marine sediments. Environ. Sci. Technol. 38, 1487–1495.

Hammerschmidt, C.R., Fitzgerald, W.F., 2008. Sediment - water exchange of methylmercury determined from shipboard benthic flux chambers. Mar. Chem. 109, 86–97.

Hammerschmidt, C.R., Fitzgerald, W.F., Balcom, P.H., Visscher, P.T., 2008. Organic matter and sulfide inhibit methylmercury production in sediments of New York/New Jersey Harbor. Mar. Chem. 109, 165–182.

Hellal, J., Guédron, S., Huguet, L., Schaefer, J., Laperche, V., Joulian, C., et al., 2015. Mercury mobilization and speciation linked to bacterial iron oxide and sulfate reduction: a column study to mimic reactive transfer in an anoxic aquifer. J. Contam. Hydrol. 180, 56–68.

Herail, G., Fornari, M., Giovani, V., Ruis, A.J., Pozzo, L., Dumont, J.F., 1991. Les placers d'or de Bolivie: Milieux de formation et structure géologique. In: IRD (Ed.), Gisements alluviaux d'or. ORSTOM, La Paz, pp. 115–143.

Hines, N.A., Brezonik, P.L., Engstrom, D.R., 2004. Sediment and porewater profiles and fluxes of mercury and methylmercury in a small seepage lake in Northern Minnesota. Environmental science & technology 38, 6610–6617.

Hollweg, T.A., Gilmour, C.C., Mason, R.P., 2009. Methylmercury production in sediments of Chesapeake Bay and the mid-Atlantic continental margin. Mar. Chem. 114, 86–101.

Huettel, M., Webster, I.T., 2001. Porewater Flow in Permeable Sediments. The Benthic Boundary Layer: Transport Processes and Biogeochemistry. pp. 144–179.

Hyacinthe, C., Anschutz, P., Carbonel, P., Jouanneau, J.M., Jorissen, F.J., 2001. Early diagenetic processes in the muddy sediments of the Bay of Biscay. Mar. Geol. 177, 111–128.

Jeong, H.Y., Klaue, B., Blum, J.D., Hayes, K.F., 2007. Sorption of mercuric ion by synthetic nanocrystalline mackinawite (FeS). Environmental science & technology 41, 7699–7705.

Kelly-Gerreyn, B.A., Hydes, D.J., Waniek, J.J., 2005. Control of the diffusive boundary layer on benthic fluxes: a model study. Mar. Ecol. Prog. Ser. 292, 61–74.

Kerin, E.J., Gilmour, C.C., Roden, E., Suzuki, M.T., Coates, J.D., Mason, R.P., 2006. Mercury methylation by dissimilatory iron-reducing bacteria. Appl. Environ. Microbiol. 72, 7919–7921.

Kostka, J.E., Luther, I.G.W., 1994. Partitioning and speciation of solid phase iron in saltmarsh sediments. Geochim. Cosmochim. Acta 58, 1701–1710.

Lanza, W.G., Acha, D., Point, D., Masbou, J., Alanoca, L., Amouroux, D., et al., 2017. Association of a specific algal group with methylmercury accumulation in periphyton of a tropical high-altitude Andean Lake. Arch. Environ. Contam. Toxicol. 1–10.

Liu, J., Valsaraj, K.T., Devai, I., DeLaune, R.D., 2008. Immobilization of aqueous Hg (II) by mackinawite (FeS). J. Hazard. Mater. 157, 432–440.

Marnette, E.C.L., Horditk, C.A., Van Breemen, N., 1992. Sulfate reduction and S-oxidation in a moorland pool sediment. Biogeochemistry 17, 123–143.

Matty, J.M., Long, D.T., 1995. Early diagenesis of mercury in the Laurentian Great Lakes. J. Great Lakes Res. 21, 574–586.

Merritt, K.A., Amirbahman, A., 2007. Mercury dynamics in sulfide-rich sediments: geochemical influence on contaminant mobilization within the Penobscot River estuary, Maine, USA. Geochim. Cosmochim. Acta 71, 929–941.

Meyers, P.A., Ishiwatari, R., 1993. The early diagenesis of organic matter in lacustrine sediments. Org. Geochem. 185–209 Springer.

Molina, C.I., Lazzaro, X., Guédron, S., Acha, D., 2018. Contaminacion de la Bahia de Cohana, Lago Titicaca (Bolivia): Desafios y oportunidades para promover su recuperacion. Ecologia en Bolivia 52, 65–76.

Monperrus, M., Gonzalez, P.R., Amouroux, D., Alonso, J.I.G., Donard, O.F.X., 2008. Evaluating the potential and limitations of double-spiking species-specific isotope dilution analysis for the accurate quantification of mercury species in different environmental matrices. Anal. Bioanal. Chem. 390, 655–666.

Paul, D., Skrzypek, G., Forizs, I.N., 2007. Normalization of measured stable isotopic compositions to isotope reference scales-a review. Rapid Communications in Mass Spectrometry: An International Journal Devoted to the Rapid Dissemination of Up-to-the-Minute Research in Mass Spectrometry 21, 3006–3014.

Perrot, V., Epov, V.N., Pastukhov, M.V., Grebenshchikova, V.I., Zouiten, C., Sonke, J.E., et al., 2010. Tracing sources and bioaccumulation of mercury in fish of Lake Baikal Angara River using Hg isotopic composition. Environmental Science & Technology 44, 8030–8037.

Point, D., Monperrus, M., Tessier, E., Amouroux, D., Chauvaud, L., Thouzeau, G., et al., 2007. Biological control of trace metal and organometal benthic fluxes in a eutrophic lagoon (Thau lagoon, Mediterranean Sea, France). Estuarine Coastal and Shelf Science 72, 457–471.

Pourchet, M., Mourguiart, P., Pinglot, J.-F., Preiss, N., Argollo, J., Wirmann, D., 1994. Sédimentation récente dans le lac Titicaca (Bolivie). C. R. Acad. Sci. Paris 319, 535–541.

Rodrigo, L.A., Wirrmann, D., 1992. II.2. General aspects of present-day sedimentation. In: Dejoux, C., Iltis, A. (Eds.), Lake Titicaca - A Synthesis of Limnological Knowledge. vol. 68. Kluwer Academic Publishers, Dordrecht/Boston/London, pp. 23–28.

Rosenthal, Y., Lam, P., Boyle, E.A., Thomson, J., 1995. Authigenic cadmium enrichments in suboxic sediments: Precipitation and postdepositional mobility. Earth Planet. Sci. Lett. 132, 99–111.

Rothenberg, S.E., Ambrose, R.F., Jay, J.A., 2008. Mercury cycling in surface water, pore water and sediments of Mugu Lagoon, CA, USA. Environ. Pollut. 154, 32–45.

Rowe, H.D., Dunbar, R.B., Mucciarone, D.A., Seltzer, G.O., Baker, P.A., Fritz, S., 2002. Insolation, moisture balance and climate change on the South American Altiplano since the Last Glacial Maximum. Clim. Chang. 52, 175–199.

Rydberg, J., Gälman, V., Renberg, I., Bindler, R., Lambertsson, L., Martinez-Cortizas, A., 2008. Assessing the stability of mercury and methylmercury in a varved lake sediment deposit. Environmental science & technology 42, 4391–4396.

Sarret, G., Guédron, S., Acha, D., Bureau, S., Arnaud-Godet, F., Tisserand, D., Goni-Urriza, M., Gassie, C., Duwig, C.l., Proux, O., Aucour, A.-M., 2019. Extreme Arsenic Bioaccumulation Factor Variability in Lake Titicaca, Bolivia. Sci. Rep. 9, 10626.

Schäfer, J., Castelle, S., Blanc, G., Dabrin, A., Masson, M., Lanceleur, L., et al., 2010. Mercury methylation in the sediments of a macrotidal estuary (Gironde Estuary, south-west France). Estuar. Coast. Shelf Sci. 90, 80–92.

Schaller, T., Moor, H.C., Wehrli, B., 1997. Sedimentary profiles of Fe, Mn, V, Cr, As and Mo as indicators of benthic redox conditions in Baldeggersee. Aquat. Sci. 59, 345–361.

Segura, H., Junquas, C., Espinoza, J.C., Vuille, M., Jauregui, Y.R., Rabatel, A., et al., 2019. New insights into the rainfall variability in the tropical Andes on seasonal and interannual time scales. Clim. Dyn. 1, 1–22.

Skyllberg, U., 2008. Competition among thiols and inorganic sulfides and polysulfides for Hg and MeHg in wetland soils and sediments under suboxic conditions: illumination of controversies and implications for MeHg net production. Journal of Geophysical Research: Biogeosciences 2005-2012, 113.

Skyllberg, U., 2012. Chemical speciation of mercury in soil and sediment. In: Liu, G., Cai, Y., O'Driscoll, N. (Eds.), Environmental Chemistry and Toxicology of Mercury. John Wiley & Sons, Inc, Hoboken, New Jersey, pp. 219–258.

Skyllberg, U., Xia, K., Bloom, P.R., Nater, E.A., Bleam, W.F., 2000. Binding of mercury(II) to reduced sulfur in soil organic matter along upland-peat soil transects. J. Environ. Qual. 29, 855–865.

Slowey, A.J., Brown, J.G.E., 2007. Transformations of mercury, iron, and sulfur during the reductive dissolution of iron oxyhydroxide by sulfide. Geochim. Cosmochim. Acta 71, 877–894.

Sunderland, E.M., Gobas, F., Branfireun, B.A., Heyes, A., 2006. Environmental controls on the speciation and distribution of mercury in coastal sediments. Mar. Chem. 102, 111–123.

Tapia, J., Audry, S., 2013. Control of early diagenesis processes on trace metal (Cu, Zn, Cd, Pb and U) and metalloid (As, Sb) behaviors in mining-and smelting-impacted lacustrine environments of the Bolivian Altiplano. Appl. Geochem. 31, 60–78.

Vairavamurthy, M.A., Manowitz, B., Maletic, D., Wolfe, H., 1997. Interactions of thiols with sedimentary particulate phase: studies of 3-mercaptopropionate in salt marsh sediments from Shelter Island, New York. Org. Geochem. 26, 577–585.

Valero-Garcès, B.L., Delgado-Huertas, A., Ratto, N., Navas, A., 1999. Large ^{13}C enrichment in primary carbonates from Andean Altiplano lakes, northwest Argentina. Earth Planet. Sci. Lett. 171, 253–266.

Wang, X., Yang, H., Gong, P., Zhao, X., Wu, G., Turner, S., et al., 2010. One century sedimentary records of polycyclic aromatic hydrocarbons, mercury and trace elements in the Qinghai Lake, Tibetan Plateau. Environ. Pollut. 158, 3065–3070.

Watras, C.J., Back, R.C., Halvorsen, S., Hudson, R.J.M., Morrison, K.A., Wente, S.P., 1998. Bioaccumulation of mercury in pelagic freshwater food webs. Sci. Tot. Environ. 219, 183–208.

Webster, R., 2001. Statistics to support soil research and their presentation. Eur. J. Soil Sci. 52, 331–340.

Weide, D.M., Fritz, S.C., Hastorf, C.A., Bruno, M.C., Baker, P.A., Guédron, S., et al., 2017. A ~6000 yr diatom record of mid-to late Holocene fluctuations in the level of Lago Winaymarca, Lake Titicaca (Peru/Bolivia). Quat. Res. 88, 179–192.